

Review

Solid Lubrication System and Its Plasma Surface Engineering: A Review

Yang Li ^{1,*} , Zelong Zhou ¹ and Yongyong He ^{2,*}

¹ School of Nuclear Equipment and Nuclear Engineering, Yantai University, Yantai 264005, China; zhouzelong20000313@163.com

² State Key Laboratory of Tribology, Tsinghua University, Beijing 100084, China

* Correspondence: metalytu@163.com (Y.L.); heyy@mail.tsinghua.edu.cn (Y.H.)

Abstract: In aerospace, aviation, nuclear power, and other high-tech fields, some essential moving parts must operate under high vacuum, high load, intense radiation, and other conditions. Under such extreme conditions, only solid lubricating materials can meet the lubrication requirements. Traditional material modification methods have problems such as high energy consumption, severe pollution, and narrow scope of application. Plasma modification technology can overcome these shortcomings. This paper focuses on several commonly used plasma preparation techniques for solid lubricating coatings, including plasma chemical heat treatment, physical vapor deposition, plasma immersion ion implantation and deposition, plasma spraying, and plasma electrolytic oxidation. Subsequently, the material systems of metal-based solid lubrication coatings are reviewed: soft metals, oxides, sulfides, nitrides, and carbon-based materials. Finally, found that the development of new solid lubricants, the improvement of existing preparation technology, and the development of new processes are the key development directions in the future.

Keywords: solid lubrication; plasma surface engineering; coatings; physical vapor deposition

1. Introduction

In industrial production and manufacturing, friction and wear are ubiquitous, and severe friction and wear will directly lead to the failure and scrap of mechanical parts [1–3]. According to statistics, the world's annual energy consumption is due to friction, accounting for about 30% of the total. More than 60% of the mechanical parts are due to severe wear and tear failure. More serious is that friction and wear will cause malignant accidents in automated facilities, resulting in losses in personnel and property [4,5]. The purpose of lubrication is to reduce the coefficient of friction and reduce wear. Standard lubrication methods include oil, grease, gas, and solid lubrication [6–8].

With the development of modern high-end equipment, the operating conditions of friction systems have become increasingly demanding. Among them, solid lubrication exhibits unique superior performance for mechanical parts that work under extreme conditions such as high temperature, high pressure, high vacuum, and high speed, as well as for some mechanical parts that cannot form hydrodynamic lubrication [9–11]. At the same time, based on the development trend of environmental protection and green manufacturing, the use of liquid lubricants is also increasingly restricted. The introduction of solid lubrication has broken the limit of oil film lubrication. Therefore, researching solid lubricating materials suitable for harsh environments has increasingly highlighted their value. Solid lubricating coatings exhibit significant advantages due to their self-lubricating function.

Solid lubrication technology is becoming a thriving field, with some layered disulfides, soft metals, graphite, diamond-like carbon films, and oxides being famous solid lubrication materials [6,12–16]. The traditional method of preparing concrete lubricating coatings has problems such as high energy consumption, severe pollution, complex operation,



Citation: Li, Y.; Zhou, Z.; He, Y. Solid Lubrication System and Its Plasma Surface Engineering: A Review. *Lubricants* **2023**, *11*, 473. <https://doi.org/10.3390/lubricants11110473>

Received: 23 September 2023

Revised: 12 October 2023

Accepted: 28 October 2023

Published: 3 November 2023



Copyright: © 2023 by the authors. Licensee MDPI, Basel, Switzerland. This article is an open access article distributed under the terms and conditions of the Creative Commons Attribution (CC BY) license (<https://creativecommons.org/licenses/by/4.0/>).

and narrow applicability. At the same time, plasma preparation technology can precisely overcome these shortcomings [17–19]. The plasma state is the fourth state of matter, a quasi-neutral gas composed of charged and neutral particles, and exhibits a collective behavior. It accounts for about 99% of cosmic significance. The modification effect of plasma on materials comes from the presence of energetic electrons, ions, and metastable, excited, and free particles in the ionized gas [20]. These particles are unstable and active, and various forms of light radiation, such as infrared radiation, accompany plasma generation. Energy particles and energy light radiation in materials are prone to desorption, doping, etching, sputtering, degradation, and cross-linking—a series of physical and chemical reactions such as interfacial polymerization.

The plasma surface treatment method involves the generation of high-energy particles that act on the surface of a material, causing chemical bonds to break and generate free radicals. These free radicals undergo cross-linking and re-bond to form a network structure, thereby improving the surface performance of the material [21,22]. By using different plasma preparation techniques and solid lubrication material system components, the lubrication performance of the coating improved to meet the needs of special working conditions [23–27]. This article elaborates on the plasma preparation methods of lubrication coatings, introduces relevant solid lubrication coating systems, and prospects for the future development trend of solid lubrication coatings.

2. Solid Lubrication Layer Plasma Surface Preparation Technology

2.1. Plasma Chemical Heat Treatment Technology

Chemical heat treatment is a heat treatment process in which a workpiece is placed in a device with an active medium, heated to a specific temperature, and maintained there [28,29]. It utilizes chemical reactions, sometimes combined with physical methods, to introduce desired elements into the surface of the workpiece, thereby altering its chemical composition, structure, and properties. The infiltration rate of plasma chemical heat treatment is faster than that of the traditional method. The deformation of the workpiece after heat treatment is small, and the composition and structure of the infiltration layer can be better controlled to obtain a high-quality infiltration layer. It has obvious advantages in energy saving and environmental protection [30–32]. There are various methods of chemical heat treatment, typically named after the infiltrated elements or compounds formed, such as nitriding [33–35], carburizing [36–38], nitrocarburizing [39], sulfurizing [40], oxidizing [41], among others.

Plasma chemical heat treatment can be divided into three stages: (1) the medium undergoes chemical decomposition at a specific temperature, generating active atoms or ions; (2) the active atoms or ions accumulate onto the workpiece; (3) the active atoms or ions diffuse from the workpiece's surface to the interior, forming a diffusion layer with a certain thickness near the surface [42–44]. The workpiece can be regarded as a unique composite material, with the interior being the original steel and the surface layer being a material infused with alloying elements. The device schematic is shown in Figure 1 [45]. By ionizing gas and bombarding the sample, nitrogen, carbon, and other ions can be injected into the material surface to improve the surface performance and properties [46–49]. Plasma nitriding/carbonitriding can increase the surface strength of the material, improve its tensile and compressive abilities, and form a compound layer of nitride or carbonitride, which can significantly reduce wear and friction [33,45,50–52]. In addition, the compound can be formed, improving the material's corrosion resistance and prolonging its service life [53–55].

Plasma sulfurizing is an effective treatment method for forming a sulfide film on the friction surface. It refers to sulfur infiltrating into the surface layer of metal parts and reacting with the metal to form sulfides through a chemical heat treatment process. Surface sulfurizing can improve the surface hardness, wear resistance, corrosion resistance, and working life of the workpiece. Plasma sulfurizing is simple, convenient to operate, cost-effective, and environmentally friendly compared to other sulfurizing processes. It can also

impart unique properties to the surface, such as high-temperature resistance, anti-biting, anti-fatigue, wear resistance, and corrosion resistance, while ensuring the toughness of the base material. Wang et al. [56,57] successfully prepared FeS lubricating film layers with low friction coefficients and good wear resistance on AISI 1045 steel, high-speed steel (M2), and die steel (L6) substrates through plasma sulfurizing. The sulfurized layer plays a role in cutting peaks and filling valleys on the surface, making the surface flatter, thus increasing the actual contact area and reducing the contact stress.

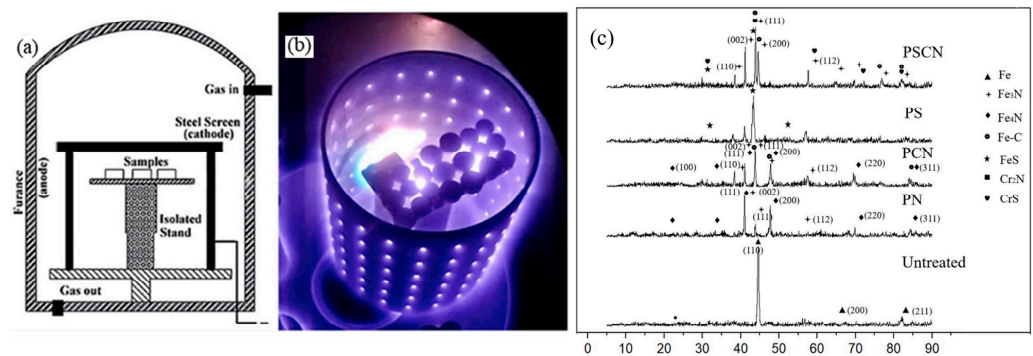


Figure 1. Schematic diagrams of the plasma chemical heat treatment furnace (a), the working hollow cathode (b), and XRD results for untreated PN, PCN, PS, and PSCN surfaces (c) [45].

Moreover, the asperities on the surface of metal materials are covered with a layer of soft sulfide, which delays the occurrence of occlusion. Han et al. [58] prepared a 3–4 μm sulfide solid lubrication layer on the surface of cobalt-based alloy coatings using laser cladding and plasma sulfurizing processes, which significantly reduced the friction coefficient and wear under dry friction conditions compared to a single cladding layer. In addition, the metal wear debris is buried in the sulfide layer or modified by the sulfide so that the abrasive wear and fatigue wear can be reduced.

Compared with traditional sulfurizing technology, low-temperature plasma sulfurizing technology has the advantages of fast sulfur infiltration speed, good layer infiltration effect, and non-toxic side effects, and has been in the surface modification of bearings, gears, molds, and other typical friction parts to achieve a wide range of industrial applications [59,60]. Sulfur infiltration technology can reduce energy and material consumption by improving the friction between moving pairs, increasing the service life and reliability of parts, and has a broad application prospect. Researchers should comprehensively apply the latest achievements in the field of computer technology, automatic control technology, and composite surface engineering technology, further promote the application of low-temperature sulfurizing technology to improve the friction situation of parts, improve the service performance and service life of equipment, and make contributions to energy saving, emission reduction, and sustainable development.

2.2. Physical Vapor Deposition (PVD) Technology

2.2.1. Magnetron Sputtering

Magnetron sputtering is a process of ionizing inert gases by applying a voltage between the cathode and anode of the furnace chamber under vacuum conditions, thereby generating a glow discharge effect [61,62]. The source of the deposited material is that Ar ions bombard the target or cathode, and the subsequent momentum transfer causes the neutral atoms of the target source to be expelled. The power supply of magnetron coating can be roughly divided into two categories: direct-current power and radio frequency power. Radio frequency power supply is particularly suitable for preparing oxide films, allowing direct use of non-conductive targets. The outstanding advantage of radio frequency over direct-current power is its ability to sputter atoms in insulating materials. Unbalanced magnetron sputtering technology increases the sputtering rate and target utilization by 30~40%. The principle is that the technology makes the magnetic field of the magnetron

sputtering target unbalanced by changing the magnetic flux, which dramatically increases the plasma density in the coating area, thereby improving the coating quality. Thin films of pure metals, alloys, and compounds can be prepared by magnetron sputtering coating equipment. The thickness can reach 5 μm . Magnets are used in magnetron sputtering on the back of the cathode to confine electrons above the target, preventing them from bombarding the substrate and allowing faster deposition rates. The principle of magnetron sputtering coating is shown in Figure 2a.

At present, the traditional magnetron sputtering has been optimized and improved by people, such as the development of various new magnetron sputtering technologies, as well as medium frequency pulse magnetron sputtering, unbalanced magnetron sputtering, radio frequency magnetron sputtering, and high power pulse magnetron sputtering (HiPIMS) [63–66].

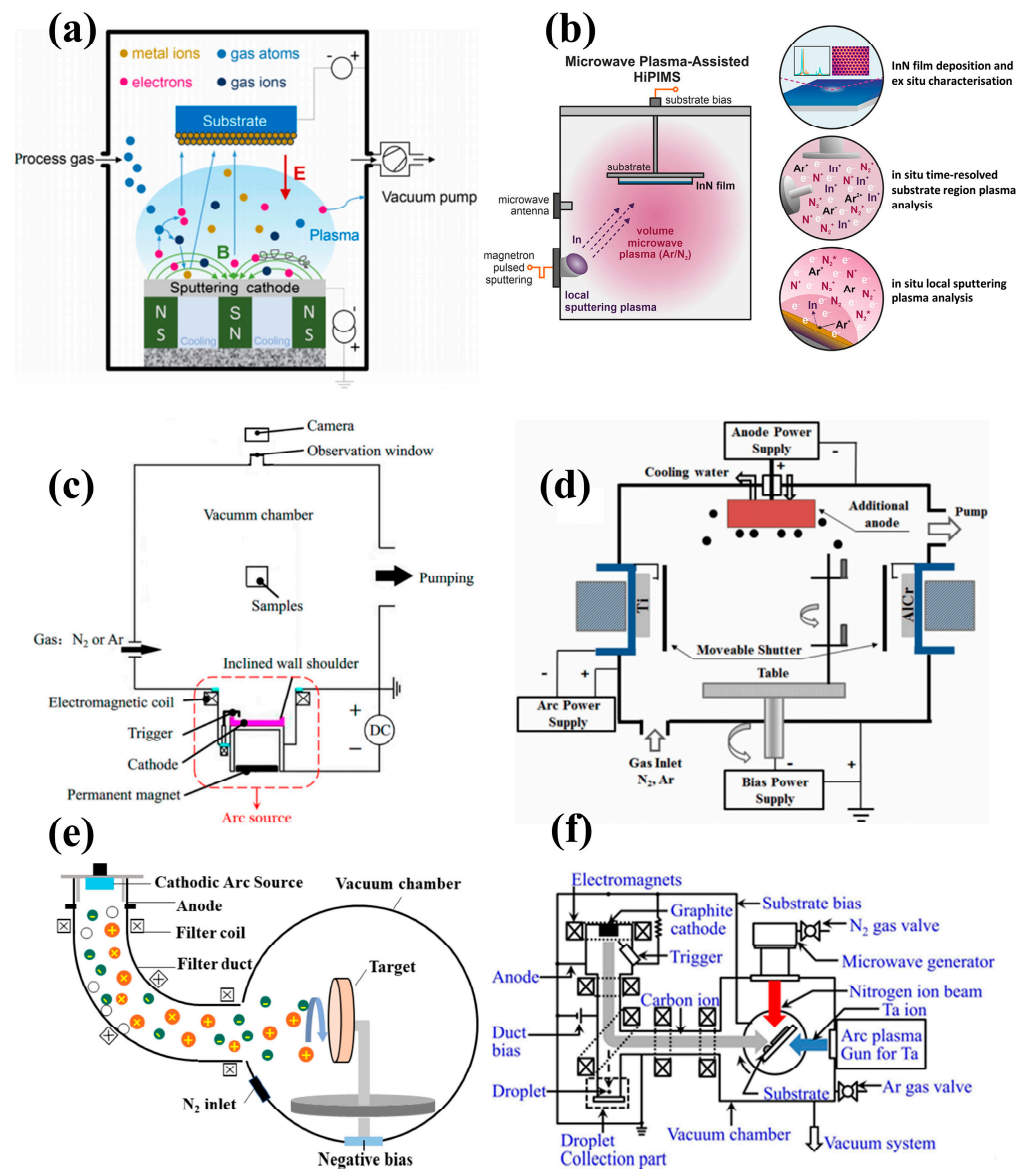


Figure 2. Mechanism schematic diagram of equipment: (a) Magnetron sputtering, (b) HiPIMS, (c) arc ion-plated, (d) multi-arc ion plating, (e) filtered cathode vacuum arc deposition, (f) ion beam assisted deposition [67–71].

HiPIMS is a relatively new magnetron sputtering deposition method. It is characterized by allowing the deposition of high-quality coatings at lower temperatures (room temperature) [72]. The reason is that the power supply used is a low-duty cycle, low-

frequency pulse power supply, which ensures a high peak current and avoids overheating of the target. The high peak current (high electron density) leads to the ionization rate of Ti by the sputtering material [73,74] as high as 90%. The large number of metal and sputtering gas ions can control the energy and flux of the growing surface-bombarding species and ensure a high energy transfer to the ever-increasing surface.

2.2.2. Arc Ion-Plated

The principle of arc ion plating (AIP) is to bombard the cathode target by arc discharge and constrain the arc with the magnetic field [75]. The cathode target acts as an evaporation source, ionizes gas molecules, ignites an arc source, forms a high-density plasma, and produces a glow discharge phenomenon [76,77]. The ionized metal positive ions collide with the reaction gas molecules and electrons. The ionized positive ions move to the surface of the workpiece under the action of the electric field, and finally, the ions are deposited on the surface of the workpiece to form a film.

Multi-arc ion plating (MAIP) combines the characteristics of evaporation and sputtering, glow discharge, and vacuum evaporation cohesively [78,79]. MAIP has the advantages of high electron ionization rate, high ion bombardment energy, and simple operation [80]. The film prepared by MAIP technology has excellent compactness and strong film-based bonding strength. However, due to the high deposition power, many large metal particles will be generated during the deposition process, causing serious particle pollution, affecting the surface roughness of the layer, and reducing the coating quality. Many scholars' studies have shown that the performance of the coating is significantly affected by different experimental parameters. The results show that the main parameters affecting the performance of the layer include target current, gas flow rate, substrate temperature, and bias voltage.

Filtered cathode vacuum arc deposition (FCVAD) is a vacuum film deposition technique using vacuum arc discharge as an evaporation source [69,81,82]. It generates ions by arc discharge on the cathode surface and carries on plasma deposition. By means of magnetic plasma filtration technology, the large particles and neutral atoms produced by the arc source are filtered out to obtain pure plasma beams, which can avoid the problems caused by large particles and bring high-quality films.

Diamond/tetrahedral amorphous carbon composite films were synthesized by a two-step preparation technique, including hot filament chemical vapor deposition (HFCVD) growth for polycrystalline diamond and subsequent FCVAD deposition for tetrahedral amorphous carbon [83]. The primary wear mechanism of the composite films in the dry friction process against ceramic Si_3N_4 ball counterpart was abrasive wear. Shen et al. [84] reported that the Ti-DLC coatings with various Ti contents were prepared by filtered cathodic vacuum arc technique by adjusting the C_2H_2 flow rate. They found that the amorphous materials show better corrosive resistant than the crystalline ones due to the absence of crystallographical effects, and the amorphous carbon would lead to the formation of a graphited lubrication layer, which can contribute to friction and inhibit corrosion.

2.2.3. Ion Beam Assisted Deposition (IBAD)

Ion beam-assisted deposition (IBAD) technology involves sputtering a target material with an ion beam composed of high-energy inert gas particles and then depositing it onto the surface of the workpiece to form a thin film [85]. This method has the advantages of low deposition temperature, good process controllability, wide adjustment range of ion energy and particle flow density, etc. [86]. Therefore, the internal stress of the prepared film is relatively small, and the adhesion between the film and the substrate is high. During the sputtering deposition of thin films, ion beams bombard a specific area on the surface of the target material, and the ion intensity distribution of the sputtering is uneven, resulting in poor thickness uniformity of the deposited film and the inability to deposit on a large area of substrate, thus significantly limiting the industrial application of large-scale models.

2.3. Plasma-Enhanced Chemical Vapor Deposition (PECVD)

PECVD is a glow-discharge chemical vapor deposition technology that uses plasma to activate. This method can reduce the opportunity temperature and control the deposition rate [87–89]. It can manufacture solid lubricant coatings with different compositions and microstructures. It allows people to change the film properties of different depths continuously. PECVD is an improvement of the traditional CVD method. In conventional CVD, heating is its activation method, thereby activating the working gas and achieving film growth. The corresponding disadvantage is that the heating step in this method may damage the deposited film. In PECVD, the technique of electron collision with working gas molecules is used to obtain the precursor required for the reaction, and the temperature of the plasma itself is not high during the response. Therefore, it can effectively avoid thermal damage. Figure 3 shows the schematic diagram of pulsed PECVD equipment and the construction of PECVD sputtering process schematic diagram.

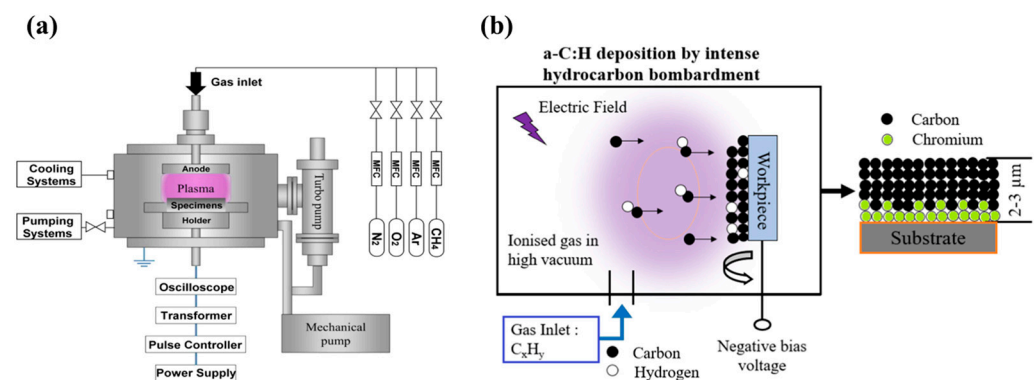


Figure 3. (a) Schematic of the DC-pulsed PECVD system, (b) Schematic construction of PECVD sputtering process [90,91].

PECVD plasma reaction is very complex. Ion bombardment causes defects on the surface, resulting in a decrease in density, and the film often contains more hydrogen. In order to improve the above shortcomings, electron cyclotron resonance (ECR) is used to strengthen the PECVD method. The gas molecules are ionized under the action of an electric field, and the plasma is formed by the strong interaction between positive and negative charges. In a low-pressure vessel, electrons can accelerate and collide with neutral molecules or atoms due to their large mean free path.

2.4. Plasma Immersion Ion Implantation and Deposition (PIII&D)

Plasma immersion ion implantation and deposition (PIII&D) is a rapidly developing new technology for material surface modification in recent years [92,93]. The outer surface of the workpiece is completely immersed in a low-pressure, high-density uniform plasma, and a high-voltage negative pulse bias voltage of several hundred Hertz and thousands to tens of thousands of volts is applied to the workpiece. The schematic diagram of the high-dose-rate PIII&D is shown in Figure 4. It overcomes the inherent directional defects of traditional methods such as thin film deposition or ion implantation and, therefore, exhibits unparalleled advantages in the surface modification process and technology of complex three-dimensional workpieces. In contrast to the above-mentioned ion-based methods, PIII uses energetic ions mostly at higher kinetic energies and in a pulsed mode. PIII&D has a series of advantages [94]: (1) The plasma beam can be injected precisely to the required depth; (2) the miscibility of the plasma beam will not occur; (3) the injected layer is a new surface layer formed by a series of physical and chemical interactions between ions and the substrate surface, and there is no stripping problem between the substrate and the new layer.

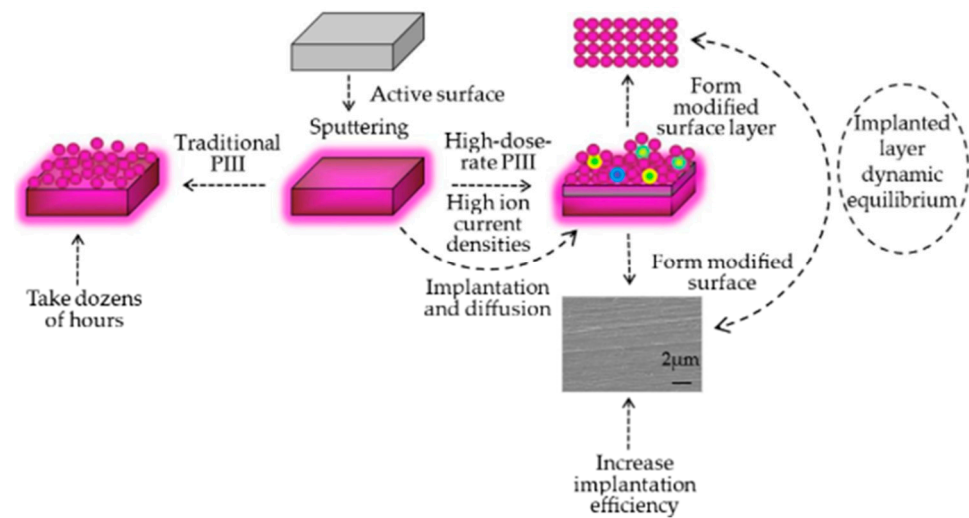


Figure 4. The schematic diagram of plasma immersion ion implantation process.

2.5. Plasma Spraying Technology

Plasma spraying technology uses a rigid non-transfer plasma arc as a heat source to heat ceramic, alloy, metal, and other powder materials to a molten or semi-molten state and then spray at high speed to the surface of the pretreated workpiece to form a firmly attached surface layer [95–97]. The working gas is ionized into plasma in the arc formed by the cathode and anode so that the powder transported from the powder port is melted or semi-melted, and the plasma is sprayed onto the substrate surface to form a coating [98]. This technology has been widely used because of its advantages, such as good coating quality, high bonding strength, various coating types, and little influence on the matrix. According to the formation of plasma medium and environmental atmosphere, it can be divided into multiple plasma spraying technologies; the most is mainly atmospheric plasma spraying and vacuum plasma spraying.

2.5.1. Atmospheric Plasma Spraying

Atmospheric plasma spraying (APS) is the earliest and most widely used technology. Ar, N₂, and H₂ are working media, and the spraying process is carried out in an atmospheric environment [99]. Among them, the process parameters are the key factors affecting the repair and strengthening quality of APS parts, so the matrix must be preheated before the parts are sprayed, about 200 °C, which has a good effect on reducing the temperature difference between the matrix and the coating and improving the bond strength. Suppose the spraying electric power and powder delivery parameters are not set appropriately. In that case, the powder composition will be destroyed, or the heating powder supply will be insufficient, resulting in low working efficiency, low bonding strength, poor coating quality, and other consequences.

2.5.2. Low-Pressure Plasma Spraying

Low-pressure plasma spraying (LPPS), also known as vacuum plasma spraying, refers to the spraying technology under the condition of a low-pressure seal controlled by the atmosphere [100], which was applied in the 1970s. Figure 5 shows the phenomenon of atmospheric plasma spraying and the microstructure of different spraying technologies and their modified layers. The principle of LPPS and ordinary plasma spraying is the same; the main difference is that the working atmosphere is a low-pressure environment, resulting in different process parameters, mainly to adapt to working in low vacuum conditions. The operating pressure is generally 4~40 kPa; in different pressure environments, we need to use other process parameters; the lower the general anxiety, the faster the particle speed. Therefore, the spraying distance can be appropriately increased to enable the spraying material to melt more thoroughly, such as the 300 ~ 350 mm spraying distance when 6.5 GPa.

Low-pressure plasma spraying, because of the uniqueness of its working atmosphere and its use in other spraying technology, cannot be processed in blank areas because it does not contact the atmosphere to avoid the shortcomings of coating oxidation and composition changes. At the same time, because of its low vacuum atmosphere characteristics, the size of the low-pressure chamber limits its spraying, so the size and shape of the processed parts are limited, and the investment is relatively significant.

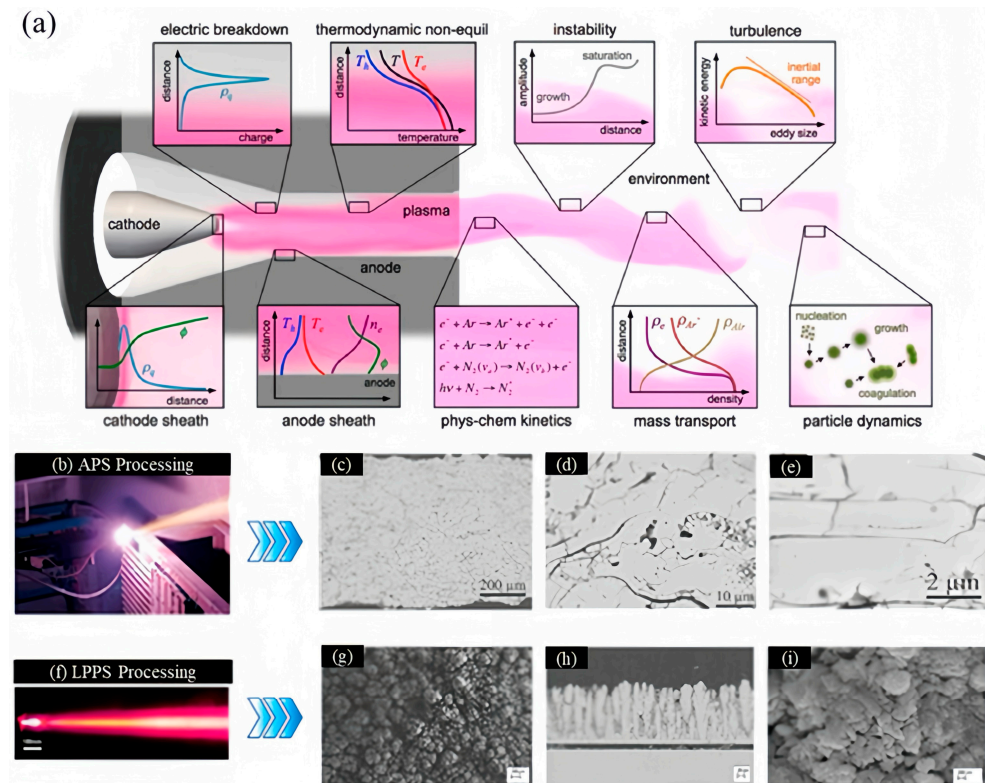


Figure 5. (a) Understanding phenomena in atmospheric plasma spraying, (b) conventional atmospheric plasma spray method, (c–e) typical microstructures of coatings, (f) low-pressure plasma spray process, (g–i) specific microstructures of coatings [101,102].

2.6. Plasma Electrolytic Oxidation

Plasma electrolytic oxidation (PEO), also known as micro-arc oxidation (MAO), is based on ordinary anodic oxidation, which further increases the working voltage to the breakdown voltage of the oxide film and causes micro-arc discharge on the surface of the metal workpiece [103–105]. Figure 6 shows the deposition process of MgO , Mg_2SiO_4 , and ZrO_2 composite coatings on bare AZ91 by PEO technology and the principle diagram of PEO technology. Various thermochemical reactions are induced by the instantaneous high temperature and high pressure generated by a micro-arc discharge, and a ceramic film mainly composed of matrix metal oxides is formed on the metal surface [106–108]. The PEO film is metallurgically bonded to the substrate with high bonding strength. At the same time, the film has excellent properties such as high hardness, corrosion resistance, and wear resistance, which can effectively improve the defects of low hardness, small elastic modulus, and poor wear resistance of the valve metal surface [109–111]. In micro-arc oxidation, electrolyte components will be introduced into the ceramic membrane. Different electrolyte compositions and electrical parameters are used, and composite membrane layers with multiple functions such as friction reduction, wear resistance, thermal barrier, and corrosion resistance can be prepared, which has a comprehensive application prospect in aerospace, equipment manufacturing, transportation, electronic appliances, and other industrial fields and is expected to produce significant economic and social benefits [103]. The basic parameters of micro-arc oxidation include voltage, current, time, electrolyte,

etc. [112–114]. Among them, the voltage and current are the main factors affecting the effect of micro-arc oxidation [115,116].

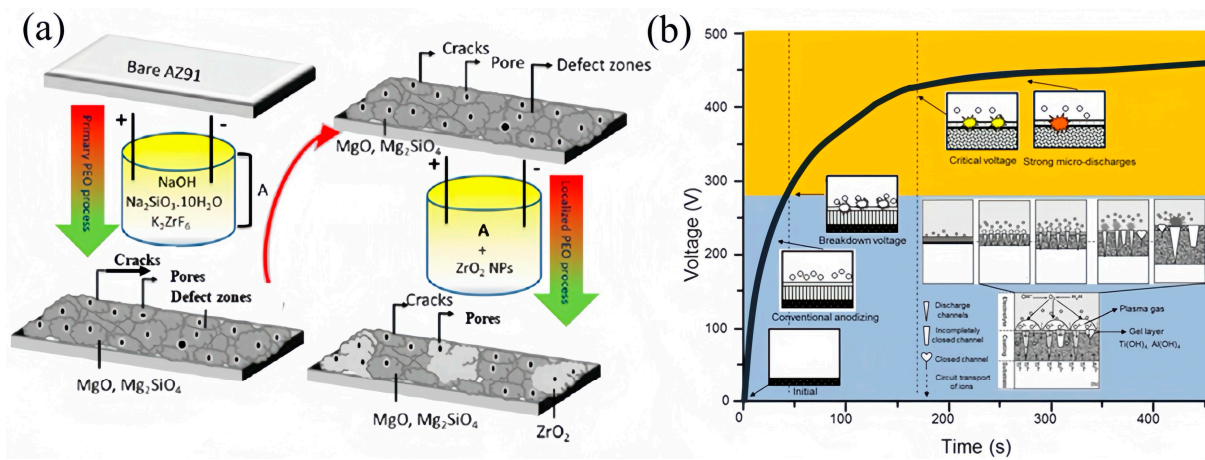


Figure 6. Schematic diagram of the PEO equipment and its coating formation process: (a) A schematic diagram of the process of preparing MgO, Mg₂SiO₄, ZrO₂ coatings on AZ91 alloy by PEO, and (b) PEO technical treatment diagram [117–119].

In recent years, research on micro-arc oxidation technology has focused on improving the process, optimizing the parameters, and studying the microstructure and properties of the ceramic layer [109,116,120,121]. Using the growth characteristics and porous characteristics of micro-arc oxidation film, researchers try to reduce the porosity of micro-arc oxidation film. Functional materials with tribological properties are introduced into the micro-arc oxidation ceramic coating to improve the surface density and minimize the friction coefficient and wear rate. Then, the micro-arc oxidation composite coating with a self-lubricating function is obtained [122]. There are two leading preparation technologies for self-lubricating micro-arc oxidation composite film: one is to make self-lubricating particles suspended or generated in electrolyte enter the growing film through electrophoresis, diffusion, and adsorption during the growth of the micro-arc oxidation ceramic film, which can be called direct composite technology. The other is that after the micro-arc oxidation ceramic film is formed, the lubricating material is introduced into the discharge micropores inside the film by post-treatment processes such as impregnation sintering, thermal spraying, magnetron sputtering, sol-gel, and electrophoretic deposition, which can be called secondary composite technology. Among them, direct hybrid technology includes solid particle addition, direct composite technology, and in-situ particle direct composite technology.

3. Solid Lubrication System

3.1. Soft Metals

Due to its low shear strength and excellent elasticity, some soft metals, including silver (Ag), lead (Pb), tin (Sn), zinc (Zn), and copper (Cu) undergo plastic deformation during sliding to adapt to the two interacting surfaces, reducing friction and wear. The friction coefficient is very sensitive to the thickness of the soft metal layer, and when the thickness is relatively thin (300–1000 nm), the obtained friction coefficient is relatively low. The mechanical properties of the metal matrix and the wear resistance of the solid lubricant are why the self-lubricating coating can significantly improve the wear resistance of the parts [123,124]. These soft metals are used as solid lubricants and can be synthesized as an alloy or employed in coatings and films using various coating techniques.

As a medium-temperature lubricant, Ag is the most widely used. Ag has a face-centered cubic structure that is prone to intergranular slip [125–127]. Ag can significantly improve the plasticity and toughness of coatings/films by refining grain size, thereby improving the tribological properties of layers [128–130]. Ag uses defects and grain boundaries

in the internal structure of the coating/film as diffusion channels and uses external temperature and friction as driving forces to diffuse towards the friction surface quickly [131]. Finally, a layer of Ag transfer film is formed on the friction contact surface to reduce the friction coefficient. A slight friction coefficient of 0.2–0.4 is maintained within its optimal film thickness range, demonstrating good lubricity.

However, several limitations restrict the use of Ag. Firstly, as a precious metal, the procurement cost of Ag is high, which poses a significant burden for large-scale applications. Additionally, the preparation and processing of Ag require complex and costly technical processes, thereby increasing the overall cost of engineering applications.

Moreover, the effectiveness of the Ag transfer film may be limited, and its durability and stability could be problematic. Under high-temperature, high-pressure, or long-term operating conditions, the Ag transfer film may be susceptible to damage or decomposition due to friction and thermal forces, thereby affecting the sustainability of its frictional properties.

In conclusion, although Ag offers advantages as a medium-temperature lubricant, factors such as its high cost, limitations in grain refinement effects, and the stability of the transfer film restrict its cost-effectiveness and reliability in engineering applications. Therefore, when considering Ag as a lubricant, it is essential to comprehensively evaluate these issues and perform thorough economic and practical assessments.

3.2. Oxides

Oxides are potentially the best choice for solid lubrication in harsh conditions, including extreme temperatures, since oxides are often structurally and chemically/thermodynamically stable. These phases, such as PVD, are usually formed in the tribo-oxidation process or used as deposition during synthesis [128]. Significant research focuses on using metal compounds, which lead to developing an oxide lubricious layer in the temperature range. Tribo-chemical reactions on the moving surface of metal friction pairs will form various oxides. Then, the oxides will participate in the process of friction and wear, which will affect the friction factor and wear form. The role of a particular class of oxides as a solid lubricant, the so-called Magneli phases in high-temperature applications, has been researched quite significantly [132]. A. Magneli [133] first discovered that Mo and W form oxides with planar faults belonging to homologous series based on the common structural principles Me_nO_{3n-1} or Me_nO_{3n-2} . These materials are sub-stoichiometric oxides of transition metals, including Mo, W, V, or Ti, with a weakly bonded lamellar microstructure leading to a favorable lubrication mechanism. Table 1 summarizes standard solid lubricated oxide coatings. Erdemir et al. [134] pointed out that the tribological properties of metal oxides are related to the ionic potential (cationic charge/cationic radius). Oxides with higher plasma potential of V_2O_5 , B_2O_3 , and Re_2O_7 have a smaller friction factor, maintaining a friction factor of 0.13–0.25. In comparison, oxides with a lower plasma potential of Al_2O_3 , ZrO_2 , and FeO have a friction factor greater than 0.5. Vanadium oxides as Magneli solid lubrication phases are reported by Franz and Mitterer, who demonstrated lubricious behavior similar to titanium oxides [135].

Although oxide coatings exhibit good tribological performance, they may experience higher friction coefficients at low temperatures. This is because the materials of the coatings tend to become more brittle in low-temperature environments, and the chemical reaction rate between interface materials slows down. As a result, lubrication is reduced, leading to increased friction on the surface of the coating. Additionally, their wear resistance may be relatively poor. Since oxide coatings are typically thin films, they are prone to wear and fatigue during long-term use, especially under high loads and intense friction conditions. This can result in a decrease in the performance of the coatings. In summary, while oxide coatings exhibit good tribological performance, their friction coefficients at low temperatures can be higher, and their wear resistance may be relatively poor. However, ongoing research and development efforts are focused on finding solutions to overcome these limitations and improve the performance of oxide coatings in low-temperature applications.

Solid solution oxides such as (Al, Cr)₂O₃ form the corundum phase in relatively low-temperature PVD processes and may be promising for low friction and wear coatings but may also be metastable at moderate temperatures [136]. W. Gulbiński et al. [137] reported that the friction coefficient of single-phase Ag₂MoO₄ coating deposited by PVD decreased with increasing temperature, from 0.35 at 100 °C to 0.25 at 500 °C. Ouyang et al. [138] reported on ZrO₂-BaCrO₄ composites solid lubricants utilizing a low-pressure plasma-sprayed technique, and they conducted tribological tests up to 800 °C. The denied oxide/graphite composite coating mainly consisted of a combination of γ -Al₂O₃, α -Al₂O₃, graphite, and amorphous alumina, which was successfully fabricated on prepared pure aluminum bulk using a one-step PEO process [139].

The performance requirements of the surface anti-friction and wear resistance for the motion components were studied from the perspective of regulating the organizational structure of coatings. Multiple electrolyte systems were developed, and lubricating coatings' formation process, structural characteristics, and tribological properties were compared. The study showed that the composite coating with nano TiO₂ grains embedded with an amorphous SiO₂ phase significantly improved the wear resistance of the titanium alloy and reduced the friction coefficient to 0.15–0.2. To further reduce the friction coefficient, solid lubricant graphite was introduced into the micro-pores and cavities on the micro-arc oxidation surface, serving as a lubricant reservoir to continuously supply graphite to the frictional surface. This approach significantly reduced the friction coefficient to 0.1 [140,141].

MoS₂/Al₂O₃ self-lubricating ceramic coatings with optimized pore structures were fabricated by in-situ synthesis of MoS₂ combined with PEO under different duty cycles [142]. The anti-friction properties of the MoS₂/Al₂O₃ coatings were improved compared to the traditional PEO coating.

Most metal oxides have better tribological properties at high temperatures but have higher friction coefficients at low temperatures. Therefore, the relationship between the tribological properties of metal oxides and the size of the ion potential can be used to explore further the tribological properties of metal oxides in low-temperature environments and increase the application of oxide-based composite coatings across a wide temperature range.

Table 1. Tribological performance of solid lubricant oxide coatings.

| No. | Coating | Material | Process | Phase Structure | Compound Layer/ μ m | Friction Pair | Load/N | COF | Refs. |
|-----|---|--------------------------------|----------------------|---|-------------------------|--------------------------------|--------|-------------|-------|
| 1 | Al ₂ O ₃ + MoS ₂ | Steel substrates | Plasma spraying | α -Al ₂ O ₃ , MoS ₂ | ~450 | SS316L | 10 | 0.21 | [143] |
| 2 | Al ₂ O ₃ + ZrO ₂ | SUS304 | Plasma spraying | Al ₂ O ₃ , ZrO ₂ | 210~300 | Al ₂ O ₃ | 10 | 0.05~0.08 | [144] |
| 3 | Al ₂ O ₃ -3TiO ₂ /CaF ₂ | | Plasma spraying | Al ₂ O ₃ , TiO ₂ , CaF ₂ | - | medium-carbon steel | 40 | 0.029~0.142 | [145] |
| 4 | Al ₂ O ₃ -40 wt% TiO ₂ | Alumina-40 wt% Titania | Plasma spraying | Al ₂ O ₃ , TiO ₂ | 500 | Si ₃ N ₄ | 20 | 0.16 | [146] |
| 5 | TiO ₂ -SiAlON | 316 stainless steel | Plasma spraying | TiO ₂ , Al ₂ O ₃ | 0.2 | Si ₃ N ₄ | 5 | 0.1 | [147] |
| 6 | ZrO ₂ -BaCrO ₄ | AISI 304 | Plasma spraying | ZrO ₂ , BaCrO ₄ | 200 | Al ₂ O ₃ | 50 | 0.3 | [138] |
| 7 | Al ₂ O ₃ + ZrO ₂ | 7075 Al alloy | PEO | ZrO ₂ , Al, Al ₂ O ₃ , α -Mg, MgZn ₂ , Y ₂ O ₃ | 14~24 | WC/Co balls | 2 | 0.22 | [148] |
| 8 | Y ₂ O ₃ + MAO | ZK60 | PEO | MgZn ₂ , Y ₂ O ₃ | 3~10 | Si ₃ N ₄ | 5 | 0.4 | [149] |
| 9 | NiCr-BaCr ₂ O ₄ | NiCr alloy | PEO | BaCr ₂ O ₄ | | Al ₂ O ₃ | 5 | 0.2 | [150] |
| 10 | MgO | Mg alloy | PEO | MgO | 10 | GCr15 | 5~15 | 0.28~0.30 | [148] |
| 11 | MgO | AZ31 Mg alloy | PEO | Mg, MgO | | ZrO ₂ | 2~6 | 0.17 | [151] |
| 12 | Ag-MoO ₃ | Al ₂ O ₃ | Magnetron sputtering | Ag ₂ MoO ₄ | | Al ₂ O ₃ | 1 | 0.2 | [137] |
| 13 | (Ag, Ta)Ox | Inconel 718 | Magnetron sputtering | AgTaO ₃ , AgTaO ₅ | 2 | Si ₃ N ₄ | 2 | 0.16 | [152] |

3.3. Nitrides

Nitride coatings mainly refer to transition metal nitrides and their binary, ternary, and multivariate derivatives. TiN and CrN series compounds are the main corrosion-resistant and wear-resistant nitride coatings because of their extremely high hardness and low friction coefficient [153–156]. Table 2 summarizes the friction of some common TiN-based and CrN-based coatings. Nitride coatings have higher mechanical properties and thermal stability than pure metal coatings. Corresponding oxides are generated during friction, providing a certain degree of overall protection. Due to the different oxidation temperatures and oxidation products of various coatings, their performance also varies [143,157]. Li et al. [158] reported that plasma nitriding (PN-480 and PN-500) and TiN coating deposition treatment (MAIP-3 and MAIP-6) were respectively performed on the surface of TA2 pure titanium. The specific results are listed in Figure 7. The tribological property of the four samples was ranked from best to worst as PN-480 > MAIP-3/6 > PN-500. The COFs of the treated samples oscillate steadily and repeatedly between 0.11 and 0.12, indicating that the friction interface is in a boundary lubrication state. The nanostructured TiN coating showed the best tribological characteristics due to a high Pb content and a texture-less state with a low grain size. This coating had a low friction coefficient (~0.1) over 50,000 test cycles.

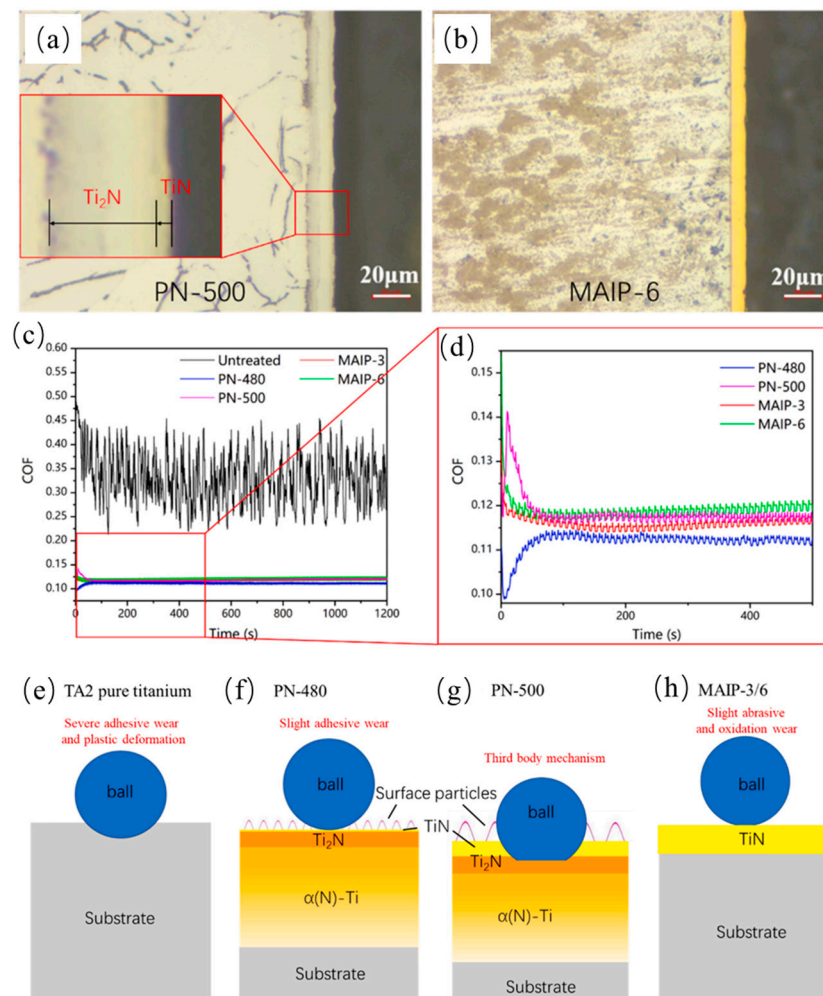


Figure 7. (a,b) Optical micrographs of cross-sections of PN and MAIP samples, (c,d) the friction curves of untreated, PN-480, PN-500, MAIP-3, and MAIP-6 samples, (e–h) schematic description for wear mechanism of different models under lubricant conditions [158].

In order to improve the lubrication performance of unit metal nitrides, many studies have shown that the comprehensive protection performance of coatings can be significantly enhanced by doping reinforcement elements into layers. Standard doping features include C, B, Si, Ni, Al, Mo, Y, W, and so on [159–165]. Doping C element in the coating can refine the grain, reduce the friction coefficient to a certain extent, and improve the wear resistance [166]. The CrBN coating [167] obtained by doping B element in the layer forms an amorphous/nanocrystal mixed structure of amorphous BN and nanocrystal CrN, which significantly improves the hardness of the CrBN coating and effectively improves the fracture toughness and elastic strain resistance of the layer. The Si element can play the dual role of refining grain and toughening, reducing the coating's friction coefficient and wear rate, and improving the lubrication performance of the layer in the liquid lubrication environment [168]. The addition of Ni can significantly strengthen the brittleness and hardness of the nitride coating and enhance the anti-crack formation ability of the coating [169]. The coating system MoN-Ag is an exciting candidate for industrial applications as a low-friction coating at elevated temperatures due to the formation of lubricious molybdenum oxides and silver molybdates. The study of ternary nitride coating is an extension of binary nitride coating, which mainly develops nitride coating with more comprehensive properties through the combination of oxidation resistance, lubrication, and load resistance nitride.

A considerable research system has been formed for high entropy alloy nitrides because of their multi-components and cocktail effect. It has good hardness, higher melting temperature, and high oxidation and wear resistance [170]. In Lin [171], (AlTiCrZrNb)N coatings with different substrate bias voltages were deposited on single crystal Si and cemented carbide substrates using arc ion plating. The lowest average friction coefficient was 0.26, and the lowest wear rate was $8.86 \pm 1.05 \times 10^{-6} \text{ mm}^3 \cdot \text{N}^{-1} \cdot \text{m}^{-1}$. The excellent mechanical properties contributed to reducing coating wear during friction and promoted the generation of surface oxide layers, which acted as a lubricant during friction. As a new research hotspot, high-entropy nitride ceramics may have a good application prospect in various structural and functional fields. However, the research in corrosion-wear coupling protection is still missing, which may be a hot spot in future service performance research of high-entropy nitride ceramic coatings.

If the nitrided coating has defects such as penetrating cracks, it is easy to peel off during friction. By designing the microstructure of the coating, the contradiction between high hardness and poor toughness of the coating can be alleviated, the generation of cracks, voids, and other defects can be reduced, and the wear resistance of the layer can be effectively improved. After years of development, the coating microstructure has gradually evolved from the traditional single-layer coating to different structures such as multilayer coating, nano-multilayer coating, nano-composite coating, and gradient coating.

The multilayer architecture can be composed of ceramic and metallic layers or two different ceramic layers [167,172–174]. The former can have both the toughness of metal and the high hardness of nitride ceramics, and the metal layer and multi-layer interface can simultaneously play a good role in inhibiting crack propagation. The latter can combine the excellent characteristics of different metal nitrides and improve the hardness and wear resistance of the coating. T. Polcar et al. [175] compared and prepared CrN and Cr/CrN coatings prepared by AIP, and the tribological properties of multilayer structures were better than those of single layers.

Elmkhah et al. [176] investigated that the effect of Cr/CrN multilayer coating on improving the tribological properties is more significant compared to CrN coating using cathode arc evaporation. Comacli [29] found that TiAlN/CrN multilayer coatings have smaller grain size, higher surface hardness, and better adhesion to the substrate, which makes the friction coefficient and wear rate significantly lower than that of the CrN and TiAlN single-layer coatings. Wang et al. [177] prepared nano-multilayer CrN/CrCN and Cr/Cr_xN and single-layer CrN and CrCN using arc ion plating technology. The excellent lubrication properties of nano-layered CrN/CrCN coating are mainly attributed to the

synergistic effect of hard Cr-C in the layer and the graphite lubrication phase formed during friction, and the excellent barrier effect of the multi-layer transverse interface on the corrosive medium in the coating microstructure. Duh [178] reported an architectural design strategy to engineer the mechanical and high-temperature tribological properties of a TiAlSiN/VSiN multilayer. The multilayer system exhibited a low friction coefficient of 0.28, which was revealed at a multilayer with a bilayer period of 16 nm during the wear test at 700 °C. The self-lubricating V₂O₅ acted as the lubricant successfully and significantly manipulated the friction coefficient during the high-temperature wearing process. The TiSiN/Ag multilayer coatings showed a significantly improved toughness compared with the TiSiN coating. The individual Ag layers of nano-multilayer coatings, not only as a self-lubricating but also as a barrier that inhibited micro cracks propagation, the formation of threading defects throughout all coatings, cause energy dissipation by passing through the interface zones without making the coating fail and at the same time prevented aggressive seawater through the micro-pores [179].

Table 2. Tribological performance of solid lubricant nitride coatings.

| No. | Coating | Material | Process | Phase Structure | Compound Layer/ μm | Friction Pair | Load/N | COF | Refs. |
|-----|--------------|---------------------------|--------------------------|------------------------|-------------------------------|--|--------|----------|-------|
| 1 | TiN | Ti6Al4V | Plasma nitriding | TiN, Ti ₂ N | - | GCr15 | 5 | 0.2~0.4 | [180] |
| 2 | TiN | Ti6Al4V | Plasma nitriding | TiN, Ti ₂ N | - | Alumina ball | 3 | 0.05~0.3 | [181] |
| 3 | TiN | Q235 steel | PECVD | TiN | 500 | AISI E52100 steel | 490 | 0.37 | [182] |
| 4 | TiN | Ti6Al4V | PECVD | TiN | 151 \pm 11 | Ti-6Al-4V | 50 | 0.44 | [183] |
| 5 | TiN | AISI 1040 | Plasma spraying | TiN | 120 | AISI O ₂ steel | 45 | 0.44 | [184] |
| 6 | TiN | 440C stainless steel | Magnetron sputtering | | 10 | alumina and aluminum | 1 | 0.3 | [185] |
| 7 | TiN | Si wafers | Magnetron sputtering | TiN | 0.75~1 | Al ₂ O ₃ | 1 | 0.1 | [186] |
| 8 | TiN | HSS M2 | Cathodic arc evaporation | TiN | >1 | WC (70%) | 2.94 | 0.38 | [184] |
| 9 | TiN | Si | HiPIMS | TiN | | Sapphire steel ball | 20 | 0.26 | [187] |
| 10 | TiSiN(Ag) | WC | HiPIMS | TiN, SiN | 2.2~2.8 | Al ₂ O ₃ , TiAl6V4 | 5 | 0.5 | [188] |
| 11 | TiAlN | WC-Co | HiPIMS | TiN, TiAlN | | Steel ball | 2 | 0.5 | [188] |
| 12 | TiAlN | HSS M2 | Magnetron sputtering | | 2.25 | WC (70%) | 2.94 | 0.42 | [189] |
| 13 | TiAlSiN/VSiN | Inconel 718 | Magnetron sputtering | | 1.2 | Al ₂ O ₃ | 1 | 0.28 | [178] |
| 14 | TiAlN/TiAl | Ti6Al4V | FCVA | | 17.13 | Si ₃ N ₄ | 20 | 0.05 | [178] |
| 15 | (TiAlCrN)C | SUS 304 | FCVA | | | Si ₃ N ₄ | 1 | 0.2~0.3 | [190] |
| 16 | TiN-W | 316L SS | Multi-arc ion plating | | 1.6 | Si ₃ N ₄ | 2 | 0.33 | [191] |
| 17 | TiMoCN | M2 | Multi arc ion plating | | 3.9 | Si ₃ N ₄ | 9.81 | 0.18 | [192] |
| 18 | TiSiN/Ag | Ti6Al4V | Arc ion plating | | 2.0 | WC + 6% Co | 5 | 0.28 | [179] |
| 19 | TiCN | HSS M2 | Cathodic arc evaporation | | >1 | 100Cr6 (20%) | 0.98 | 0.24 | [184] |
| 20 | Ti-Cr-B-N | Si (100) wafer/hard alloy | Cathodic arc evaporation | | 0.6 | WC + 6% Co | 5 | 0.45 | [193] |
| 21 | Ti-Si-B-N | Si (100) wafer/hard alloy | Cathodic arc-evaporation | | 1.5 | WC + 6% Co | 5 | 0.39 | [193] |
| 22 | Ti-Al-Si-B-N | Si (100) wafer/hard alloy | Cathodic arc evaporation | | | WC + 6% Co | 5 | 0.39 | [193] |
| 23 | CrN | 316L | Multi-arc ion plating | CrN | | SiC | 5 | 0.37 | [194] |
| 24 | CrN | 304 SS | Cathode arc evaporation | CrN | 2.0 | Al ₂ O ₃ | 2 | 0.52 | [176] |
| 25 | CrN | 440a | Cathodic arc deposition | CrN | 25 \pm 1 | Al ₂ O ₃ | 5 | 0.39 | [195] |
| 26 | Cr/CrN | AISI 304 | Cathode arc evaporation | Cr CrN | 1.3 | Al ₂ O ₃ | 2 | 0.46 | [176] |
| 27 | CrN | WC-Co | FCVA | CrN | 2 | Si ₃ N ₄ | 5 | 0.35 | [196] |
| 28 | CrAlSiN | 304 | FCVA | | 0.9 | ZrO | 1 | 0.46 | [197] |

Table 2. Cont.

| No. | Coating | Material | Process | Phase Structure | Compound Layer/ μm | Friction Pair | Load/N | COF | Refs. |
|-----|---------------------------|-------------------|----------------------------|--|-------------------------------|--------------------------------|--------|------------|-------|
| 29 | CrN/CrAlN | 430 | Arc ion plating | CrN | 3.29 | Al ₂ O ₃ | 10 | 0.3 | [198] |
| 30 | CrN/MoN/MoS | nconel 718 alloyI | Magnetron sputtering | CrN Mo ₂ N MoS ₂ | 3.93 | Al ₂ O ₃ | 2 | 0.3 | [199] |
| 31 | (CrAlTiNbV)N _x | AISI 440C | Magnetron sputtering | | 0.8 | AISI 440C | 20 | 0.096 | [200] |
| 32 | (CrAlTiNbV)N _x | 9Cr18 | Magnetron sputtering | | 0.6~0.83 | 9Cr18 | 20 | 0.06 | [201] |
| 33 | MoN-Ag | | Magnetron Sputtering | δ -MoN Mo γ -Mo ₂ N | 1.7~2.4 | Al ₂ O ₃ | 10 | 0.23~0.26 | [200] |
| 34 | MoAlTiN | 17-4 PH | Cathodic arc evaporation | AlTiN Mo ₂ N | 5.6 | WC-6Co | 10 | 0.28 | [202] |
| 35 | Mo-S-N | AISI 316 | Plasma-assisted deposition | Mo ₂ S ₃ Mo ₃ S ₄ MoS ₂ | 1 | WC/Co | 2 | 0.05~0.28 | [203] |
| 36 | Mo-Se-N | S600 | Direct current Sputtering | | | WC/Co | 45 | 0.22~0.015 | [163] |
| 37 | MoN-Ag | HSS M2 | HiPIMS | MoN, MoAg _x | 2 | Al ₂ O ₃ | 10 | ~0.25 | [204] |
| 38 | W-S-N | 100Cr6 | Magnetron sputtering | | 2.3 | 100Cr6 | 55.8 | 0.003 | [205] |
| 39 | AlTiSiN + TiSiN | 316LVM | Magnetron sputtering | TiN TiSiN AlCrN CrN | 11.30 | Al ₂ O ₃ | 30 | 0.11 | [206] |
| 40 | (AlTiCrZrNb)N | YG6 | Arc ion plating | | 2.07 | Si ₃ N ₄ | 2 | 0.26 | [171] |

Nanostructured coatings are coatings whose structure or components are controlled at the nanoscale. For example, a nanostructured coating with hard TiAlN as the substrate MoS and lubricating film is prepared by controlling PVD parameters. The superlattice coating is an extension of the multi-layer, multi-component coating, which means that the thickness of each single layer in the coating is between 1 and 50 nm. This structure significantly improves the coating's hardness, properties, and bonding strength, thereby improving the friction and wear performance. Gradient coatings are also an extension of multilayer multicomponent coatings, meaning that each layer in the coating is functionally graded and periodically arranged. Intelligent coating is a new concept, which means that the coating can change with the application conditions or external environment to meet the use requirements of particular settings.

3.4. Sulfides

There are many solid lubricating materials, and sulfides are an essential and common type. The most common solid lubricating materials are MoS₂, FeS, and WS₂ [48,207–209]. Standard preparation techniques for sulfide solid lubricating coatings include plasma spraying and PVD. With the continuous improvement of surface treatment equipment, new composite preparation techniques have emerged, such as laser cladding surface treatment, non-equilibrium magnetron sputtering, and plasma-enhanced chemical vapor deposition. Sulfide coatings are porous, allowing them to store and retain lubricating media, making them widely applicable to various friction surfaces. Sulfurizing treatment can result in a sulfur-rich layer containing solid lubricating phases on the surface of the workpiece, significantly improving the anti-friction performance of different materials. Table 3 shows the research progress of several common solid lubricating coatings.

FeS has a close-packed hexagonal structure like graphite. It has the characteristics of low hardness, low resistance to deformation, plastic solid flow ability, and low shear strength. Under the action of frictional force, it easily slips along the lattice plane and moves to the mating surface, reducing direct contact between the metal matrix and thereby reducing the friction coefficient and improving wear resistance [210–213]. FeS has a porous

structure with small-capillary effects, which can absorb lubricating oil to form a stable oil film. During the mixed lubrication friction process, when the lubricating oil film on the mating surface becomes thin or damaged, more lubricating oil can be provided to the surface, maintaining an excellent anti-friction effect. FeS has a simple and low-cost preparation process, making it widely used in industrial production with good development prospects [214]. Figure 8 shows the FES coatings prepared by ion infiltration and plasma spraying technology respectively and their tribological properties. In addition, it also shows the anti-friction and anti-adhesion mechanism of the bearing just after infiltration.

FeS can be formed at lower temperatures, but when the processing temperature increases, FeS₂ is generated, which is detrimental to the material's wear resistance. FeS₂ has a different structure from FeS. It has a cubic crystal system, higher hardness, and higher friction coefficient and shear strength. Therefore, if the processing temperature is too high, it will lead to a higher amount of FeS₂ generated in the material, which decreases the material's wear resistance. Therefore, proper control of the processing temperature to ensure the formation of sufficient FeS and minimize the generation of FeS₂ is crucial for maintaining good wear resistance of FeS materials.

MoS₂ is also a layered hexagonal crystal structure material [215–217]. The layers consist of S-Mo-S three-atomic-layer structures held together by weak van der Waals forces between the layers [194,218–220]. In the occurrence of sliding, the crystalline layers of MoS₂ will easily slide and orient parallel to the direction of relative movement, which provides the lubricating effect [209,221–223]. On the other hand, the solid ionic bond between S and Mo provides the lamellae a high resistance to asperities penetration.

WS₂ has a hexagonal lattice structure and is an essential lubricating material [224]. It is suitable for lubrication under normal and harsh conditions such as high temperature, high pressure, high vacuum, high load, radiation, and corrosive media [225,226].

Because of the small shear strength of the solid lubricating film, it plays a good role in lubricating the friction surface between hard metals, and the contact area between friction pairs has not increased significantly. Due to the low shear strength of the coated solid lubricating film, it has a specific adhesion to the friction surface. In the process of friction, the solid lubricating film coated on the substrate surface is easily transferred to the surface of the dual material, forming a transfer film. In this way, friction can occur between the transfer film and the lubricating film, which reduces the friction coefficient and effectively protects the conflict. The three sulfides also exhibit distinct characteristics. FeS has a higher friction coefficient compared to MoS₂ and WS₂. MoS₂ offers an extraordinarily low friction coefficient. However, the pure MoS₂ lubricating film is challenging to employ for prolonged periods in ambient air, particularly under humid conditions, due to its tendency to oxidize and form MoO₃, thus diminishing the lifespan of the MoS₂ lubricating film. In comparison, WS₂ possesses a higher oxidative resistance temperature in ambient air and exhibits superior adaptability to specific high-temperature environments.

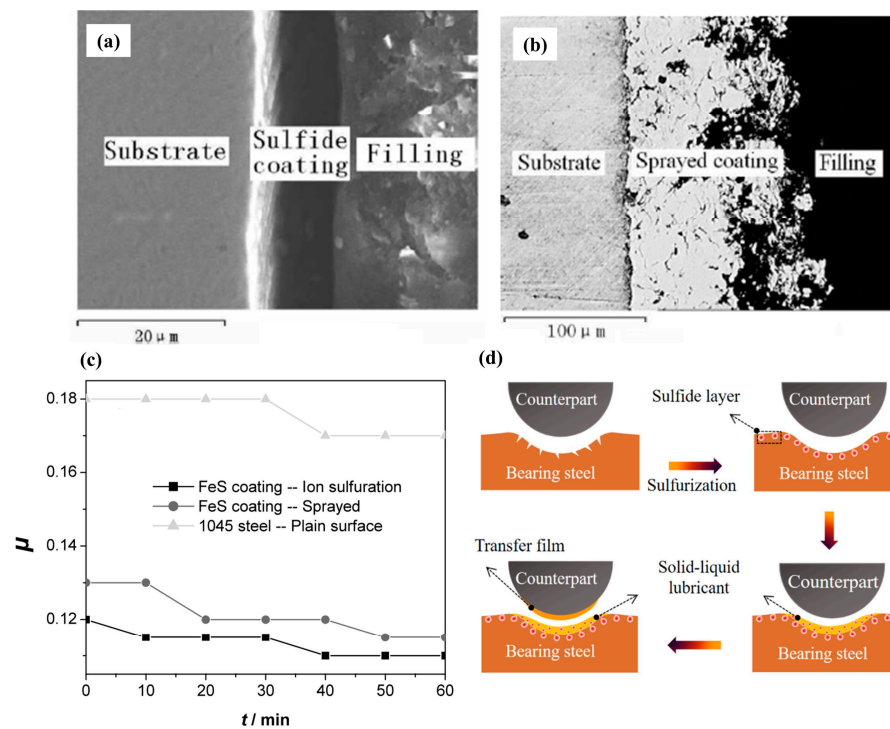


Figure 8. Cross-section morphologies. (a) Ion sulfurized coating, (b) sprayed FeS coating, (c) tribological properties of the two kinds of FeS coatings friction coefficient, (d) anti-friction and anti-adhesion mechanism of the bearing steel after sulfurization [227,228].

Table 3. Tribological performance of solid lubricant sulfide coatings.

| No. | Coating | Material | Process | Compound Layer/ μm | Friction Pair | Load/N | COF | Refs. |
|-----|-----------------------------------|----------------------------------|----------------------|-------------------------------|--|--------|-----------|-------|
| 1 | MoS ₂ | AISI 52100 | Magnetron sputtering | 0.9 | | | 0.08 | [229] |
| 2 | MoS ₂ | CF170 steel | Magnetron sputtering | 1.4 | SiC | 5 | 0.056 | [230] |
| 3 | MoS ₂ | Monocrystalline silicon | PECVD | 0.6 | 9Cr18 | 3 | 0.025 | [231] |
| 4 | MoS ₂ -V | AISI 440 C steels | Magnetron Sputtering | 1~2 | AISI 440 C | 3 | 0.04 | [231] |
| 5 | MoS ₂ /WS ₂ | 304 stainless steel and silicon | Magnetron sputtering | 2.5~3 | GCr15 | 5 | 0.08 | [232] |
| 5 | FeS | 35CrMo steel | Plasma sulfurizing | 0.1 | AISI 52100 | 10 | 0.12 | [233] |
| 7 | FeS | Ni-based alloy | Plasma sulfurizing | 3~4 | 1045 steel | 50 | 0.03~0.05 | [234] |
| 8 | FeS | AISI 4135 | Plasma sulfurizing | 10 | AISI 52100 | 200 | 0.03~0.04 | [235] |
| 9 | FeS | AISI 1045 steel | Plasma spraying | 800 | 52100 steel | 70 | | [236] |
| 10 | FeS | St12 steel | Plasma electrolysis | | AISI 52100 | | 0.2 | [237] |
| 11 | FeS/MoS ₂ | CoCrFeMoNi high entropy alloy | Plasma sulfurizing | 5 | GCr15 | 50 | 0.15 | [231] |
| 12 | WS ₂ | AISI 440C stainless steel | Magnetron sputtering | | AISI 440C stainless steel | | 0.03~0.05 | [238] |
| 13 | WS ₂ | 1045 steel | Plasma spraying | | AISI 52100 steel | 5 | | [239] |
| 14 | WS ₂ | 3Cr13 martensite stainless steel | Magnetron sputtering | | GCr15 | 0.5 | 0.06 | [240] |
| 15 | WS ₂ | Si | Magnetron sputtering | | Si ₃ N ₄ ceramic balls | 0.49 | 0~0.3 | [241] |

3.5. Carbon-Based Coatings

As a multifunctional solution, carbon-based solid lubricant coatings have received significant attention in various industrial applications for reducing friction and wear problems. These coatings are typically composed of carbon elements such as graphite and graphene. These carbon elements can form a molecular slip layer on the friction surface, reducing the interaction between the characters and reducing friction and wear [242,243]. Carbon-based coatings can adsorb and disperse small particles, such as metal particles, forming a protective layer between the friction surfaces and reducing direct contact and wear. Additionally, carbon-based coatings may gradually release self-lubricating particles during the friction process, reducing the coefficient of friction and further decreasing friction and wear. These coatings also can prevent oxidation and chemical reactions, protecting the substrate from the oxidation and corrosion caused by the friction surface [244], thereby reducing wear. Standard carbon-based solid lubricant coatings include.

3.5.1. Graphite Coating

As a carbon-based solid lubricating material, graphite coating has excellent anti-wear properties [245]. In graphite coatings, carbon atoms form a hexagonal honeycomb structure in a specific arrangement [242,246]. Graphite exhibits a layered structure, and the interaction between graphite layers is mainly driven by van der Waals forces, which are weak attractions [243,247]. These van der Waals forces allow the graphite layers to slide relative to each other in the plane, resulting in the lubricating properties of graphite.

Graphene is an ultra-thin two-dimensional carbon material with a single-layer thickness of only 0.335 nm. The carbon atoms are densely arranged in a sp^2 hybridization in a two-dimensional hexagonal structure, forming a honeycomb lattice structure. This structure gives graphene unique thermal, electrical, mechanical, and tribological properties, such as high fracture strength and toughness, easy shear spreading, etc. Compared to graphite, the larger specific surface area and ultra-thin layered structure allow graphene to adhere more easily to frictional surfaces, making it a friction material with great potential for applications.

PECVD is a commonly used method for preparing graphite coatings. In this method, plasma and chemical vapor are used as a mixture, producing thin films with a thickness of micrometers without the need for solvents and without damaging the material. This method allows the initiation of chemical reactions through discharge in a gas environment, further activating the CVD process. It is evident that compared to other ways, it can form more uniform films and has characteristics such as low deposition temperature, fast coating speed, control over coating thickness, and hydrophobic/hydrophilic properties of the material surface. Graphite coatings prepared by PECVD can reduce the wear rate of the substrate by more than twice [248].

3.5.2. Diamond-like Carbon Coatings

The molecular structure of diamond-like carbon coatings (DLC coatings) is usually amorphous or nanocrystalline, which means that their system is not an ordered crystalline structure but more random and irregular. DLC coatings mainly comprise carbon and hydrogen atoms, forming carbon-hydrogen and carbon-carbon bonds. Carbon atoms in DLC coatings exist in sp^2 and sp^3 bonds and are a metastable form of amorphous carbon without an explicit lattice structure. Therefore, DLC coatings have excellent properties of both diamond and graphite. The performance of the coating depends on the ratio of sp^2 bonds to sp^3 bonds. The higher the percentage of sp^2 bonds in the layer, the more graphitized the coating is, resulting in better self-lubricating properties and lower friction coefficient. Still, the hardness will decrease, and the film resembles graphite. The higher the ratio of sp^3 bonds in the coating, the higher the hardness of the film, and the performance is closer to natural diamond [249]. The connectivity and distribution of these bonds will affect the properties of the coating, such as hardness and lubricity.

The different preparation processes also lead to differences in the performance of DLC coatings [250–253]. It can be observed from Figure 9 that the surface morphology and friction coefficient of DLC films prepared by different processes differ greatly. DLC coatings prepared by PECVD HiPIMS exhibit other tribological properties. DLC coatings prepared by PECVD on ion-nitrided substrates exhibit the best tribological performance, with the highest SP3 ratio and the highest H/E ratio. They demonstrate an overall failure mode of delamination. Through dual treatment of active screen plasma nitriding and PECVD, the adhesion of DLC amorphous hydrogenated carbon coatings can be significantly improved, and the critical load can reach 15 N [254].

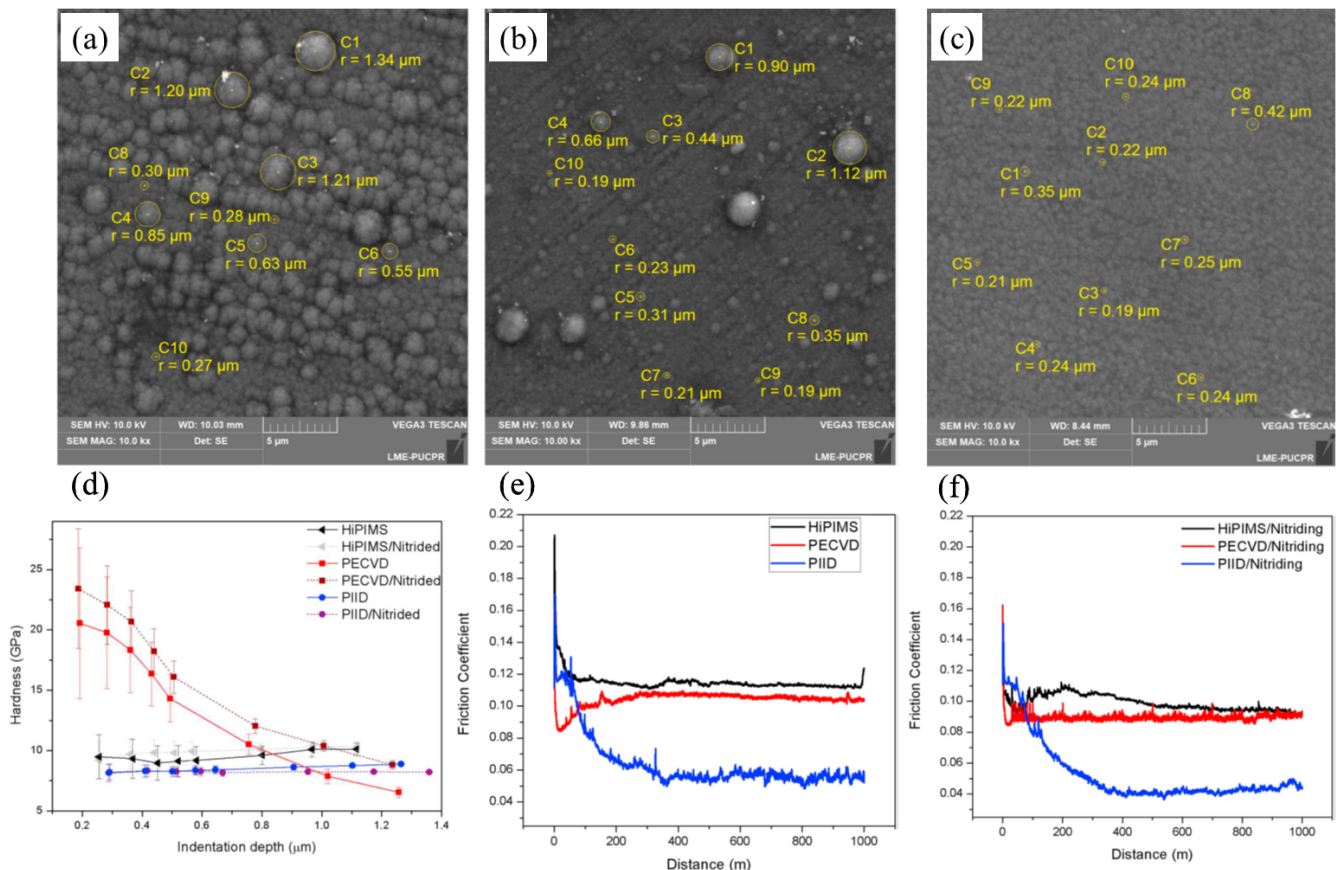


Figure 9. The aspect of the steel surfaces coated with DLC by (a) HiPIMS, (b) PECVD, and (c) PIID, (d) the hardness of DLC coatings, (e) the friction coefficient of DLC on un-nitrided steel, (f) The friction coefficient of DLC on nitrided steel [250].

There is no widely accepted view on the friction and wear mechanism of DLC films. The more representative theories are graphitization theory, chemical adsorption/passivation dangling bond theory, and transfer film theory. These three mechanisms often interact with each other. The graphitization theory suggests that the debris is usually graphitized or stored in grooves during the wear process of DLC films. The chemical adsorption/passivation dangling bond theory proposes that when oxygen, hydrogen, and water molecules are present, the carbon atoms on the film's surface are passivated, and the degree of covalent bond interaction becomes less noticeable. Even if some bonds are exposed, the adsorbed molecules will quickly decompose them, resulting in low friction. The transfer film theory suggests that when DLC films are in frictional contact with materials of high hardness, during the frictional process, they will transform from a diamond-like structure to amorphous carbon rather than graphite. The amorphous carbon will then transfer to the counterpart to form a transfer film, reducing the coefficient of friction.

Non-metallic elements doped into DLC films bond with carbon atoms, changing the sp^3/sp^2 ratio and causing subtle structural changes, thereby improving thermal stability and tribological performance [255,256]. With the addition of metals into DLC films, the doped elements are incorporated into the amorphous carbon's crosslinked network in the form of solid solutions, nanocrystals, or carbides, forming a nanocrystalline/amorphous composite structure [84,257–259]. In Figure 10, the friction coefficient and wear mechanism of Cr-doped DLC film can be observed.

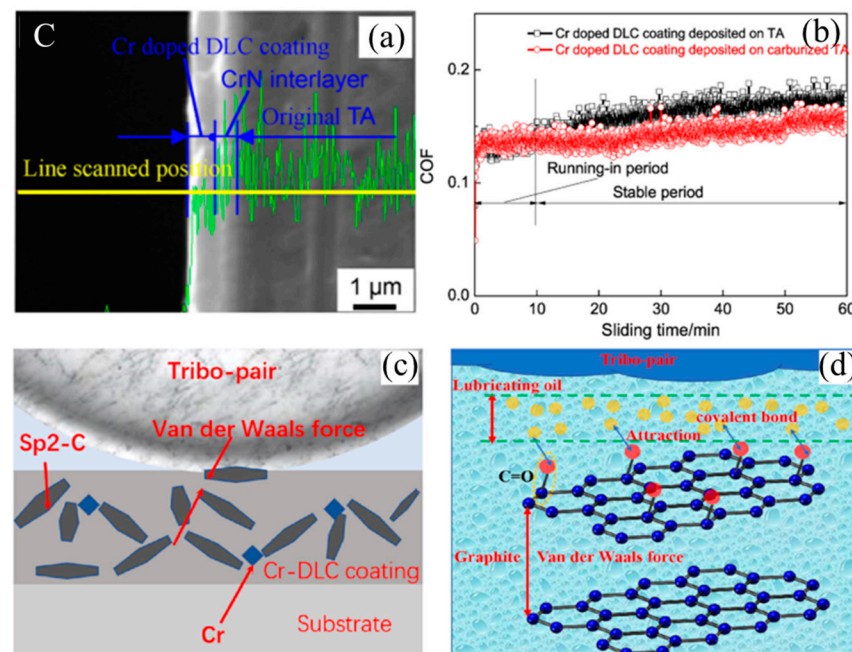


Figure 10. (a) Line scan analysis of Cr doped DLC coating, (b) COFs of Cr doped DLC coatings, (c,d) wear models of Cr doped DLC coatings under friction-lubrication and oil-lubrication conditions [260].

The research on the tribological properties of DLC coatings doped with other different elements is shown in the following Table 4.

Li et al. [256] used plasma-enhanced chemical vapor deposition to prepare Si-DLC multilayer coatings with different modulation periods. The friction and wear performance of the coatings were measured in an air environment. It was found that the friction coefficient of the multilayer silicon-DLC coating was very low (~ 0.05) after running-in in the air. The low friction in the air was attributed to the deep grooves capturing the wear debris and the formation of a Si-rich transfer layer on the counter surface. M. Evaristo et al. [261] evaluated the tribological performance of DLC coatings alloyed with different elements and found no direct relationship between friction and wear. The third body formed on the sliding surface significantly impacted the system's tribological performance. Figure 11 demonstrates the influence of different element doping on the friction coefficient of DLC thin films.

Table 4. Tribological performance of diamond-like carbon coatings.

| No. | Coating | Material | Process | Phase Structure | Compound Layer/ μm | Friction Pair | Load/N | COF | Refs. |
|-----|---------|----------------------|----------------------|------------------------------------|-------------------------------|---------------|--------|------------|-------|
| 1 | DLC | TiB ₂ | Magnetron sputtering | SP ³ &SP ² C | ~ 0.5 | WC | 5 | 0.2 | [262] |
| 2 | DLC | 304 stainless steel | Magnetron sputtering | SP ³ &SP ² C | | 100Cr6 | 1 | ~ 0.2 | [263] |
| 3 | DLC | Polished steel disks | Magnetron sputtering | SP ³ &SP ² C | 2.2 | 100Cr6 steel | 5 | 0.15 | [261] |

Table 4. Cont.

| No. | Coating | Material | Process | Phase Structure | Compound Layer/ μm | Friction Pair | Load/N | COF | Refs. |
|-----|-----------------------|----------------------|---------------------------------|-----------------------------------|-------------------------------|--------------------------------|--------|-------------|-------|
| 3 | DLC | AISI 4140 | HiPIMS | SP3&SP2 C | 3 | Al ₂ O ₃ | 10 | ~0.12 | [250] |
| 5 | DLC | AISI 4140 | PECVD | SP3&SP2 C | 7 | Al ₂ O ₃ | 10 | ~0.10 | [250] |
| 6 | DLC | AISI 4140 | Plasma ion immersion deposition | SP3&SP2 C | 7 | Al ₂ O ₃ | 10 | ~0.05 | [250] |
| 7 | DLC | AISI 304L | FCVA | SP3&SP2 C | 3~13 | 100Cr6 | 20 | 0.8 | [264] |
| 8 | Ti-DLC | AISI 304L | FCVA | SP3&SP2 C | | Si ₃ N ₄ | 2 | 0.028~0.087 | [84] |
| 9 | W-DLC | Polished steel disks | Magnetron sputtering | SP3&SP2 C, W | 1.4 | 100Cr6 steel | 5 | 0.43 | [261] |
| 10 | W-DLC | M2 tool steel | Magnetron sputtering, PECVD | SP3&SP2 C, WC | | Diamond | 0.5 | 0.07~0.09 | [265] |
| 11 | WS ₂ -DLC | TiB ₂ | Magnetron sputtering | SP3&SP2 C, WS ₂ | ~0.5 | WC | 5 | 0.05 | [262] |
| 12 | Ag-DLC | Polished steel disks | Magnetron sputtering | SP3&SP2 C, Ag | 1.2 | 100Cr6 steel | 5 | 0.23 | [261] |
| 13 | Si-DLC | M2 tool steel | PECVD | SP3&SP2 C, SiC | | Diamond | 0.5 | 0.08~0.11 | [265] |
| 14 | Si-DLC | Polished steel disks | Magnetron sputtering | SP3&SP2 C, Si | 1.4 | 100Cr6 steel | 5 | 0.09~0.12 | [261] |
| 15 | SiO-DLC | Polished steel disks | Magnetron sputtering | SP3&SP2 C, SiO | 1.4 | 100Cr6 steel | 5 | 0.09~0.12 | [261] |
| 16 | Ne-DLC | AISI D2 | HiPIMS | SP3&SP2 C | | | | 0.001 | [266] |
| 17 | Cu Nanoparticles-DLC | 304L Stainless steel | Magnetron sputtering | SP3&SP2 C, Cu | 5.2 | GCr15 | 100 | ~0.13 | [267] |
| 18 | S-F-DLC | 304 stainless steel | PECVD | SP3&SP2 C, F, S | 2 | GCr15 | 1 | 0.01~0.02 | [268] |
| 19 | H-DLC | AISI-52100 steel | PECVD | SP3&SP2 C | 1 | AISI-52100 steel | 10 | 0.12~0.15 | [269] |
| 20 | Ta/TaN/Ta(C,N)/Ta-DLC | Cemented carbide | Arc ion plating, HiPIMS | TaN, TaC, SP3&SP2 C | 1.22 | Al ₂ O ₃ | 5 | 0.15 | [270] |
| 21 | Ti/(Cu, MoS)-DLC | 304 stainless steel | Magnetron sputtering | SP3&SP2 C, MoS ₂ , CuO | | SiC | 5 | 0.036~0.064 | [271] |

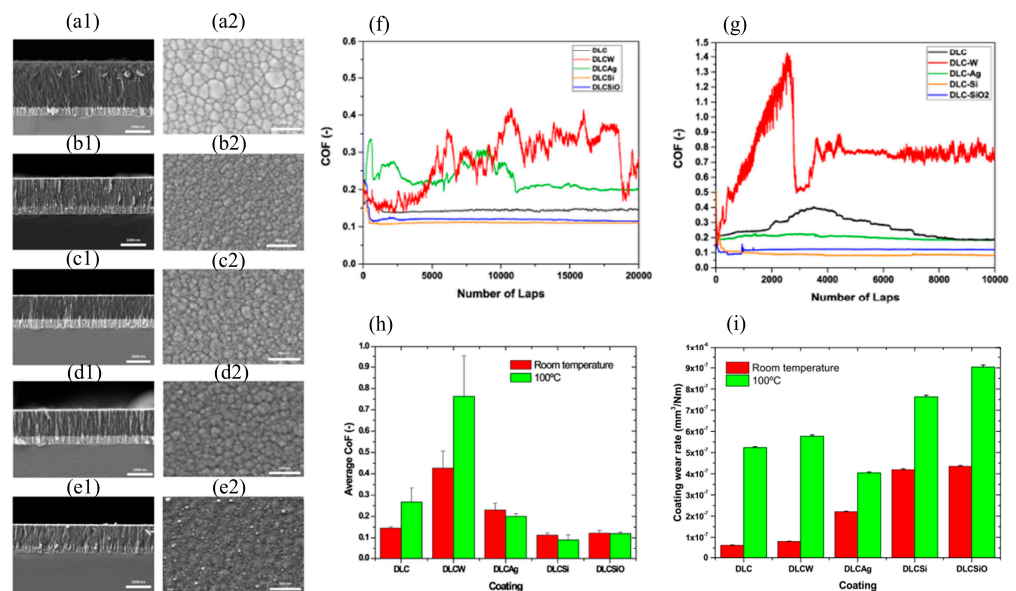


Figure 11. SEM images of the cross-section and surface (a1,a2) DLC, (b1,b2) W-DLC, (c1,c2) Si-DLC, (d1,d2) SiO-DLC, (e1,e2) Ag-DLC, respectively. Tribological characterization friction behavior of pin-on-disk tests with steel balls: (f) friction curves at room temperature for all coatings, (g) friction curves for all layers when tested at 100 °C, (h) average friction for all coatings at room temperature and 100 °C, (i) specific wear rate at room temperature and 100 °C of coatings tribological tested against steel balls [261].

3.5.3. Graphene Thin Film

Graphene is a two-dimensional material with a single atomic thickness [272]. Due to its unique electronic, electrical, mechanical, and thermal properties, it has attracted significant attention in many fields [273,274]. In addition, graphene is also an excellent solid lubricant. Compared with other solid lubricants, graphene has strong wear resistance in various test environments and does not cause any adverse effects. In addition, its derivatives are graphene oxide, fluorinated graphene, and graphene-based composite films. When graphene is used as a lubricating additive, under the action of pressure and shear, the graphene with a higher degree of exfoliation overlaps and changes in an orderly manner and will revert to a layered friction film parallel to the sliding direction [275].

In addition to its excellent properties, graphene can significantly improve its tribological properties when combined with other anti-friction and wear-resistant materials. The wrinkled structure of graphene is beneficial to the growth of nano-copper. The combination of graphene and silver is easy to agglomerate, affecting the weak interface bonding and slightly reducing the wear. The TiC/graphene composite film deposited on titanium foil by the PECVD method maintained a high yield strength after annealing [276]. The combination of graphene and WC/Co can reduce the friction coefficient by about 30 %, but the wear resistance is poor. This is because graphene forms a lubricating film on the WC surface, but it is challenging to create a large-scale continuous lubricating film after being worn out by the wear debris [277].

3.5.4. Fullerene-like Coatings

In amorphous carbon-based thin films, it is generally believed that the high hardness of the film comes from sp³ bonding, while an increase in sp² adhesion leads to a softer film. However, highly crosslinked sp² hybridized carbon forms a three-dimensional hybridized network structure in FLC thin films, resulting in high hardness and film elasticity. Due to the shorter sp² bonding in the graphite-like planes than the sp³ bonding in diamond, single-layer graphene slides and deforms under external forces, embedding it in the amorphous network structure. This amorphous network composite structure gives the film an ultra-low friction coefficient, even reaching super lubricity.

Fluorinated fullerene films were prepared using high-frequency pulsed plasma-enhanced chemical vapor deposition technology, and the fluorine content was controlled by changing the CF₄/CH₄ ratio [278]. It was found that when the fluorine content is low, the primary carbon sites bond with adjacent carbon atoms, forming a short-range ordered fullerene-like structure. C-F and C-CF bonds gradually accumulate with the increase in fluorine content, and CF₂ groups appear in the carbon matrix. These fluorine groups terminate the carbon network and reduce the formation of large carbon rings and chains, making the fullerene structure short-range disordered. As the atomic fraction of fluorine increases from 4.8% to 15.5%, the corresponding steady-state friction coefficient gradually increases from 0.052 to 0.175. At the same time, the wear rate and depth are positively correlated with the fluorine content [279]. To further study the effect of nitrogen content, direct current magnetron sputtering technology was used to introduce nitrogen gas at controlled ratios of 13% to 19% (denoted as 1CN_x, 2CN_x, . . . , 7CN_x) [280]. The highest elastic modulus (94%, 92%) and hardness (21 GPa, 20 GPa) were obtained in 3CN_x and 4CN_x. The linear fitting of the measured friction coefficient results shows that the decrease of friction coefficient in samples 3CN_x and 4CN_x is related to the increase of sp³ bond and C-N hybridization, elastic modulus and recovery rate. The increase of friction coefficient in sample 7CN_x is related to the decrease of nitrogen atom percentage. Hydrogen doping is the most common method for studying fullerene thin films, using techniques such as chemical vapor deposition and magnetron sputtering [281]. A series of FL-C: H films were prepared for research by introducing CH₄ at a flow rate of 10 mL/min and varying H₂ flow rates at 0, 2.5, 5, 7.5, and 10 mL/min [282]. The H₂ flow rate significantly influences the evolution of the FL structure. When there are more odd-numbered rings, the film exhibits lower friction coefficients, and a higher fraction of odd-numbered calls indicates a higher FL structure

content. The lowest friction coefficient and wear were achieved when the H₂ flow rate was 5 mL/min. By combining plasma nitriding technology with PECVD, iron elements can be introduced into the steel substrate during coating deposition, and the Fe elements are uniformly distributed in the FL-C: H film, significantly improving its anti-friction and wear-resistant properties [283].

4. Conclusions

Plasma surface engineering technology has many advantages over other technologies, such as low processing temperature, environmental friendliness, and excellent surface properties with fewer materials. It has apparent effects of energy saving, material saving, and pollution reduction. In today's context of scarce resources and increasing environmental pollution, the development of plasma surface engineering will gain new opportunities and vitality. Therefore, research can be conducted from the following three aspects.

- Deeply explore the self-lubricating mechanism of coatings, significantly the current carrying tribological performance mechanism of coatings under harsh working conditions, further optimize the quality of coatings, integrate existing lubrication materials, processes, and test results, and use computer simulation technology to provide lubrication solutions for different needs and working conditions.
- The plasma preparation process of solid lubrication coatings is becoming increasingly prosperous and advanced, and different process methods can be selected according to additional requirements. Duplex techniques often lead to performance breakthroughs, such as combining multi-arc ion plating and magnetron sputtering, plasma chemical heat treatments, and magnetron sputtering.
- The development of gradient functional coatings and self-healing coatings has initially formed a system, and intelligent solid lubrication coatings have also shown hope in recent research, leading to developments in the lubrication field.

Author Contributions: Writing—review and editing, Y.L.; Writing—original draft, Z.Z.; Supervision, Y.H. All authors have read and agreed to the published version of the manuscript.

Funding: This research was funded by the National Natural Science Foundation of China, grant number 52175192.

Data Availability Statement: The data presented in this study are available on request from the corresponding author.

Acknowledgments: Thanks for the technical assistance from the state key laboratory of tribology in advanced equipment. We would like to express our heartfelt gratitude to Lu Jinpeng, Yan Jiwen, Dou Haichun, and Wang Zhengwei for their invaluable support in data collection.

Conflicts of Interest: The authors declare no conflict of interest.

References

1. Meng, Y.G.; Xu, J.; Jin, Z.M.; Prakash, B.; Hu, Y.Z. A review of recent advances in tribology. *Friction* **2020**, *8*, 221–300. [[CrossRef](#)]
2. Holmberg, K.; Erdemir, A. Influence of tribology on global energy consumption, costs and emissions. *Friction* **2017**, *5*, 263–284. [[CrossRef](#)]
3. Scharf, T.W.; Prasad, S.V. Solid lubricants: A review. *J. Mater. Sci.* **2013**, *48*, 511–531. [[CrossRef](#)]
4. Pawlus, P.; Koszela, W.; Reizer, R. Surface Texturing of Cylinder Liners: A Review. *Materials* **2022**, *15*, 8629. [[CrossRef](#)] [[PubMed](#)]
5. Ramezani, M.; Ripin, Z.M.; Jiang, C.-P.; Pasang, T. Superlubricity of Materials: Progress, Potential, and Challenges. *Materials* **2023**, *16*, 5145. [[CrossRef](#)] [[PubMed](#)]
6. Zhao, J.; He, Y.Y.; Wang, Y.F.; Wang, W.; Yan, L.; Luo, J.B. An investigation on the tribological properties of multilayer graphene and MoS₂ nanosheets as additives used in hydraulic applications. *Tribol. Int.* **2016**, *97*, 14–20. [[CrossRef](#)]
7. Ma, L.R.; Zhang, C.H.; Liu, S.H. Progress in experimental study of aqueous lubrication. *Chin. Sci. Bull.* **2012**, *57*, 2062–2069. [[CrossRef](#)]
8. Guo, J.; Si, Y.; Liu, Q.; Cao, X.; Cheng, J.; Yang, J.; Liu, W. The lubrication regimes and transition laws of gallium liquid-metal. *Tribol. Int.* **2023**, *188*, 108838. [[CrossRef](#)]
9. Kumar, R.; Hussainova, I.; Rahmani, R.; Antonov, M. Solid Lubrication at High-Temperatures—A Review. *Materials* **2022**, *15*, 1695. [[CrossRef](#)]

10. Qi, W.; Wang, W.; Zong, R.; Yang, X.; Yang, Y. Evolution of the structure and properties of (Zr_{1-x}Hf_x)B₂ solid solution ceramics from first-principle theory. *Vacuum* **2022**, *203*, 111283. [[CrossRef](#)]
11. de Mello, J.D.B.; Juste, K.C.; Kapsa, P.; Binder, C.; Klein, A.N. Influence of Surface Finishing on the Tribological Behavior of Self-Lubricating Iron-Based Composites. *Tribol. Trans.* **2018**, *61*, 560–568. [[CrossRef](#)]
12. Xia, Y.; Lu, Y.; Yang, G.; Chen, C.; Hu, X.; Song, H.; Deng, L.; Wang, Y.; Yi, J.; Wang, B. Application of Nano-Crystalline Diamond in Tribology. *Materials* **2023**, *16*, 2710. [[CrossRef](#)] [[PubMed](#)]
13. Goyal, D.; Dang, R.K.; Goyal, T.; Saxena, K.K.; Mohammed, K.A.; Dixit, S. Graphene: A Path-Breaking Discovery for Energy Storage and Sustainability. *Materials* **2022**, *15*, 6241. [[CrossRef](#)] [[PubMed](#)]
14. Bakhtiari-Zamani, H.; Saebnoori, E.; Bakhsheshi-Rad, H.R.; Berto, F. Corrosion and Wear Behavior of TiO₂/TiN Duplex Coatings on Titanium by Plasma Electrolytic Oxidation and Gas Nitriding. *Materials* **2022**, *15*, 8300. [[CrossRef](#)]
15. Liu, X.Y.; Cai, W.M.; Zhang, Y.; Wang, L.Q.; Wang, J.J. Tuning microstructure and mechanical and wear resistance of ZrNbTiMo refractory high-entropy alloy films via sputtering power. *Front. Mater.* **2023**, *10*, 1145631. [[CrossRef](#)]
16. Rosenkranz, A.; Costa, H.L.; Baykara, M.Z.; Martini, A. Synergetic effects of surface texturing and solid lubricants to tailor friction and wear—A review. *Tribol. Int.* **2021**, *155*, 106792. [[CrossRef](#)]
17. Sevilla, P.; Gseibat, M.; Peláez, J.; Suárez, M.J.; López-Suárez, C. Effect of Surface Treatments with Low-Pressure Plasma on the Adhesion of Zirconia. *Materials* **2023**, *16*, 6055. [[CrossRef](#)]
18. Mitelea, I.; Bordeasă, I.; Belin, C.; Uțu, I.-D.; Crăciunescu, C.M. Cavitation Resistance, Microstructure, and Surface Topography of Plasma Nitrided Nimonic 80 A Alloy. *Materials* **2022**, *15*, 6654. [[CrossRef](#)]
19. Rotich, S.K.; Kipkirui, N.G.; Lin, T.-T.; Chen, S.-H. Effect of Varying Plasma Powers on High-Temperature Applications of Plasma-Sprayed Al_{0.5}CoCrFeNi₂Ti_{0.5} Coatings. *Materials* **2022**, *15*, 7198. [[CrossRef](#)]
20. Kusano, R.; Kusano, Y. Hybrid Plasmas for Materials Processing. *Materials* **2023**, *16*, 4013. [[CrossRef](#)]
21. Li, H.; Wang, H.; Wang, S.; Yang, Y.; Niu, Y.; Zhu, S.; Wang, F. Structure and Wear Performance of a Titanium Alloy by Using Low-Temperature Plasma Oxy-Nitriding. *Materials* **2023**, *16*, 3609. [[CrossRef](#)] [[PubMed](#)]
22. Fraçzek, T.; Prusak, R.; Ogórek, M.; Skuza, Z. Nitriding of 316L Steel in a Glow Discharge Plasma. *Materials* **2022**, *15*, 3081. [[CrossRef](#)] [[PubMed](#)]
23. Trebuňová, M.; Kottfer, D.; Kyziol, K.; Kaňuchová, M.; Medved', D.; Džunda, R.; Kianicová, M.; Rusinko, L.; Breznická, A.; Csatáryová, M. The WC and CrC Coatings Deposited from Carbonyls Using PE CVD Method—Structure and Properties. *Materials* **2023**, *16*, 5044. [[CrossRef](#)] [[PubMed](#)]
24. Grigoriev, S.; Peretyagin, N.; Apelfeld, A.; Smirnov, A.; Morozov, A.; Torskaya, E.; Volosova, M.; Yanushevich, O.; Yarygin, N.; Krikheli, N.; et al. Investigation of Tribological Characteristics of PEO Coatings Formed on Ti6Al4V Titanium Alloy in Electrolytes with Graphene Oxide Additives. *Materials* **2023**, *16*, 3928. [[CrossRef](#)] [[PubMed](#)]
25. Geng, Z.; Zhang, M.; Zhu, J.; Peng, Y.; Zhang, W.; Liu, F. Effect of Chromium Carbide Addition on the Microstructures and Properties in Dual Carbide Phases Reinforced Ni-Based Composite Coatings by Plasma Cladding. *Materials* **2023**, *16*, 4580. [[CrossRef](#)]
26. Bai, H.; Li, J.; Gao, J.; Ni, J.; Bai, Y.; Jian, J.; Zhao, L.; Bai, B.; Cai, Z.; He, J.; et al. Comparison of CrN Coatings Prepared Using High-Power Impulse Magnetron Sputtering and Direct Current Magnetron Sputtering. *Materials* **2023**, *16*, 6303. [[CrossRef](#)]
27. Drouet, M.; Le Bourhis, E. Low Temperature Nitriding of Metal Alloys for Surface Mechanical Performance. *Materials* **2023**, *16*, 4704. [[CrossRef](#)]
28. Jégou, S.; Teodorescu, M.; Barrallier, L.; Guittonneau, F. Influence of oxidizing and Nitriding parameters on nitrogen concentration of electrical steels. *Mater. Charact.* **2021**, *182*, 111529. [[CrossRef](#)]
29. Wolowicz-Korecka, E. Modeling methods for gas quenching, low-pressure carburizing and low-pressure nitriding. *Eng. Struct.* **2018**, *177*, 489–505. [[CrossRef](#)]
30. Wang, F.; Wu, J. (Eds.) Chapter 19—New advances in low-temperature plasma chemical heat treatment. In *Modern Ion Plating Technology*; Elsevier: Amsterdam, The Netherlands, 2023; pp. 475–495.
31. Li, Y.; Wang, Z.; Wang, L. Surface properties of nitrided layer on AISI 316L austenitic stainless steel produced by high temperature plasma nitriding in short time. *Appl. Surf. Sci.* **2014**, *298*, 243–250. [[CrossRef](#)]
32. Dong, H. S-phase surface engineering of Fe-Cr, Co-Cr and Ni-Cr alloys. *Int. Mater. Rev.* **2010**, *55*, 65–98. [[CrossRef](#)]
33. Shi, T.; Sun, J.-Q.; Wang, X.-W.; He, Q.-K.; Si, J.-W.; Wang, D.-R.; Xie, K.; Li, W.-S. Effect of trace water in ammonia on breaking passive film of stainless steel during gas nitriding. *Vacuum* **2022**, *202*, 111216. [[CrossRef](#)]
34. Li, Y.; He, Y.; Wang, W.; Mao, J.; Zhang, L.; Zhu, Y.; Ye, Q. Plasma Nitriding of AISI 304 Stainless Steel in Cathodic and Floating Electric Potential: Influence on Morphology, Chemical Characteristics and Tribological Behavior. *J. Mater. Eng. Perform.* **2018**, *27*, 948–960. [[CrossRef](#)]
35. Zhang, Z.; Bi, Y.; Zhang, M.; Li, Y.; Zhao, F.; Zhang, S.; He, Y. Properties of stainless-steel surface after hollow cathode assisted plasma nitriding. *Mater. Res. Express* **2020**, *7*, 116524. [[CrossRef](#)]
36. Sun, Y. Tribocorrosion behavior of low temperature plasma carburized stainless steel. *Surf. Coat. Technol.* **2013**, *228*, S342–S348. [[CrossRef](#)]
37. Hoja, S.; Klumper-Westkamp, H.; Steinbacher, M. Carbonitriding of Forging Dies. *Metals* **2021**, *11*, 1651. [[CrossRef](#)]

38. Lamim, T.D.; Pigosso, T.; Andrioni, T.D.; Martinez, D.M.; de Mello, J.D.B.; Klein, A.N.; Bendo, T.; Binder, C. Growth of Fe₃C-VACNT surfaces by metal dusting under plasma carburizing: Fractional factorial study and correlation with morphological and structural aspects. *Surf. Coat. Technol.* **2023**, *469*, 129788. [[CrossRef](#)]
39. Cisquini, P.; Ramos, S.V.; Lins, V.F.C.; Franco, A.R.; Vieira, E.A. Micro-abrasive wear resistance of the duplex expanded austenite layer phases produced by plasma nitrocarburizing. *Wear* **2019**, *436–437*, 203039. [[CrossRef](#)]
40. Cui, G.; Han, B.; Yang, Y.; Wang, Y.; Hu, C. Microstructure and tribological property of CoCrFeMoNi High entropy alloy treated by ion sulfurization. *J. Mater. Res. Technol.* **2020**, *9*, 2598–2609. [[CrossRef](#)]
41. Ghahramanzadeh Asl, H. Investigation of friction and wear performance on oxidized Ti6Al4V alloy at different temperatures by plasma oxidation method under ambient air and vacuum conditions. *Vacuum* **2020**, *180*, 109578. [[CrossRef](#)]
42. Ding, H.; Jiang, S.; Xu, J. Effect of chemical heat treatment on cavitation erosion resistance of stainless steel. *Proc. Inst. Mech. Eng. Part J J. Eng. Tribol.* **2019**, *233*, 1753–1762. [[CrossRef](#)]
43. Hoja, S.; Baustert, R.; Hasselbruch, H.; Steinbacher, M.; Fechte-Heinen, R. Investigation of combined surface treatments and coatings to increase the wear behavior of heat treatable steels. *Surf. Coat. Technol.* **2023**, *472*, 129929. [[CrossRef](#)]
44. Reger, M.; Horvath, R.; Szell, A.; Reti, T.; Gonda, V.; Felde, I. The Relationship between Surface and In-Depth Hardness for the Nitrocarburizing Treatment Process. *Metals* **2021**, *11*, 812. [[CrossRef](#)]
45. Zhang, M.; Chen, J.; Li, Y.; Chen, G.; He, Y.; Luo, J. Study on microstructural and tribological properties of sulphitrocarburized layers diffused by hollow cathode discharging. *Vacuum* **2020**, *174*, 109188. [[CrossRef](#)]
46. Li, Y.; Zhang, S.-Z.; Qiu, J.-X.; He, Y.-Y.; Xiu, J.-J.; Ye, Q.-W.; Liu, Z.-L. Effect of Electric Potentials on Microstructure, Corrosion and Wear Characteristic of the Nitrided Layer Prepared on 2Cr13 Stainless Steel by Plasma Nitriding. *Acta Metall. Sin. (Engl. Lett.)* **2018**, *32*, 733–745. [[CrossRef](#)]
47. Sumiya, K.; Tokuyama, S.; Nishimoto, A.; Fukui, J.; Nishiyama, A. Application of Active-Screen Plasma Nitriding to an Austenitic Stainless Steel Small-Diameter Thin Pipe. *Metals* **2021**, *11*, 366. [[CrossRef](#)]
48. Grützmacher, P.G.; Schranz, M.; Hsu, C.-J.; Bernardi, J.; Steiger-Thirsfeld, A.; Hensgen, L.; Rodríguez Ripoll, M.; Gachot, C. Solid lubricity of WS₂ and Bi₂S₃ coatings deposited by plasma spraying and air spraying. *Surf. Coat. Technol.* **2022**, *446*, 128772. [[CrossRef](#)]
49. Yang, Y.; Dai, X.Z.; Yang, X.R.; Zhang, S.H.; Li, D.Y. First-principles analysis on the role of rare-earth doping in affecting nitrogen adsorption and diffusion at Fe surface towards clarified catalytic diffusion mechanism in nitriding. *Acta Mater.* **2020**, *196*, 347–354. [[CrossRef](#)]
50. Li, Y.; Bi, Y.; Zhang, M.; Zhang, S.; Gao, X.; Zhang, Z.; He, Y. Hollow cathodic plasma source nitriding of AISI 4140 steel. *Surf. Eng.* **2020**, *37*, 351–359. [[CrossRef](#)]
51. Luo, Q.; Oluwafemi, O.; Kitchen, M.; Yang, S. Tribological properties and wear mechanisms of DC pulse plasma nitrided austenitic stainless steel in dry reciprocating sliding tests. *Wear* **2017**, *376–377*, 1640–1651. [[CrossRef](#)]
52. Yang, J.Q.; Le, K.; Chen, H.; Zhao, X.; Xie, X.D.; Luo, Y.; Xu, S.S.; Liu, W.M. The Significantly Enhanced Mechanical and Tribological Performances of the Dual Plasma Nitrided and PVD Coated Ti6Al4V Alloy. *Int. J. Precis. Eng. Manuf.* **2023**, *24*, 607–619. [[CrossRef](#)]
53. Li, Y.; Zhou, Z.; Yi, X.; Yan, J.; Xiu, J.; Fang, D.; Shao, M.; Ren, P.; He, Y.; Qiu, J. Improved seawater corrosion resistance of electron beam melting Ti6Al4V titanium alloy by plasma nitriding. *Vacuum* **2023**, *216*, 112463. [[CrossRef](#)]
54. Sitzmann, A.; Hoja, S.; Schurer, S.; Tobie, T.; Stahl, K. Deep nitriding-contact and bending strength of gears with increased nitriding hardening depth FIIN-D-21-00056. *J. Eng. Res.* **2021**, *86*, 649–659.
55. Li, Y.; He, Y.; Xiu, J.; Wang, W.; Zhu, Y.; Hu, B. Wear and corrosion properties of AISI 420 martensitic stainless steel treated by active screen plasma nitriding. *Surf. Coat. Technol.* **2017**, *329*, 184–192. [[CrossRef](#)]
56. Wang, H.-D.; Xu, B.-S.; Liu, J.-J.; Zhuang, D.-M. The friction-reduction model of the iron sulfide film prepared by plasma source ion sulfuration. *Surf. Coat. Technol.* **2007**, *201*, 5236–5239. [[CrossRef](#)]
57. Wang, G.-d.; Zhuang, D.-m.; Wang, K.-l.; Liu, J.-j. The comparison on tribological properties of ion sulfuration steels under oil lubrication. *Mater. Lett.* **2003**, *57*, 2225–2232.
58. Cui, G.; Han, B.; Zhao, J.; Yang, Z. Microstructure and tribological performance of sulfurizing layer prepared on the laser cladding Co-based alloy coating. *Surf. Coat. Technol.* **2017**, *331*, 27–34. [[CrossRef](#)]
59. Wang, H.-D.; Zhuang, D.-M.; Wang, K.-L.; Liu, J.-J. Anti-scuffing properties of ion sulfide layers on three hard steels. *Wear* **2002**, *253*, 1207–1213. [[CrossRef](#)]
60. Ning, Z.; Zhuang, D.-M.; Liu, J.-J.; Fang, X.-D.; Guan, M.-X.G. Wear mechanism of ion-sulphurization layer on steel under dry conditions. *Wear* **2001**, *247*, 1–8. [[CrossRef](#)]
61. Ma, Y.; Li, L.; Qian, J.; Qu, W.; Luo, R.; Wu, F.; Chen, R. Materials and structure engineering by magnetron sputtering for advanced lithium batteries. *Energy Storag. Mater.* **2021**, *39*, 203–224. [[CrossRef](#)]
62. Ju, H.; Yu, D.; Xu, J.; Yu, L.; Zuo, B.; Geng, Y.; Huang, T.; Shao, L.; Ren, L.; Du, C.; et al. Crystal structure and tribological properties of ZrAlMoN composite films deposited by magnetron sputtering. *Mater. Chem. Phys.* **2019**, *230*, 347–354. [[CrossRef](#)]
63. Luo, Q.; Yang, S.; Cooke, K.E. Hybrid HIPIMS and DC magnetron sputtering deposition of TiN coatings: Deposition rate, structure and tribological properties. *Surf. Coat. Technol.* **2013**, *236*, 13–21. [[CrossRef](#)]
64. Mei, H.; Luo, Q.; Huang, X.; Ding, J.C.; Zhang, T.F.; Wang, Q. Influence of lubricious oxides formation on the tribological behavior of Mo-V-Cu-N coatings deposited by HIPIMS. *Surf. Coat. Technol.* **2019**, *358*, 947–957. [[CrossRef](#)]

65. Li, Z.Q.; Xu, M.L.; Zhang, H.H.; He, W.F.; Zhang, G.A.; Lu, Z.B. Effect of silicon-doping on the wide-temperature tribological behavior and lubrication mechanism of WC/a-C film. *Wear* **2023**, *516*, 204614. [[CrossRef](#)]
66. Liu, Z.L.; Li, H.; Li, J.L.; Huang, J.W.; Kong, J.; Xiong, D.S. Tribological Properties Improvement of Mo-Alloyed HfN Films with a High H/E Ratio at Elevated Temperatures. *J. Tribol.-Trans. Asme* **2021**, *143*, 011704. [[CrossRef](#)]
67. Tokoroyama, T.; Tagami, Y.; Murashima, M.; Lee, W.Y.; Umehara, N.; Kousaka, H. Tribological Property of ta-CN_x:Ta Deposited via Ion Beam Assisted-Filtered Arc Deposition. *Tribol. Int.* **2022**, *168*, 107450. [[CrossRef](#)]
68. Deng, Y.; Chen, W.; Li, B.; Wang, C.; Kuang, T.; Li, Y. Physical vapor deposition technology for coated cutting tools: A review. *Ceram. Int.* **2020**, *46*, 18373–18390. [[CrossRef](#)]
69. Zhang, Z.; Zhang, L.; Yuan, H.; Qiu, M.; Zhang, X.; Liao, B.; Zhang, F.; Ouyang, X. Tribological Behaviors of Super-Hard TiAlN Coatings Deposited by Filtered Cathode Vacuum Arc Deposition. *Materials* **2022**, *15*, 2236. [[CrossRef](#)]
70. Wang, S.; Lin, Z.; Qiao, H.; Ba, D.; Zhu, L. Influence of a Scanning Radial Magnetic Field on Macroparticle Reduction of Arc Ion-Plated Films. *Coatings* **2018**, *8*, 49. [[CrossRef](#)]
71. Hain, C.; Schweizer, P.; Sturm, P.; Borzi, A.; Thomet, J.E.; Michler, J.; Hessler-Wyser, A.; Nelis, T. Microwave plasma-assisted reactive HiPIMS of InN films: Plasma environment and material characterisation. *Surf. Coat. Technol.* **2023**, *454*, 129188. [[CrossRef](#)]
72. Hovsepian, P.E.; Ehiasarian, A.P. Six strategies to produce application tailored nanoscale multilayer structured PVD coatings by conventional and High Power Impulse Magnetron Sputtering (HIPIMS). *Thin Solid Films* **2019**, *688*, 137409. [[CrossRef](#)]
73. Alami, J.; Maric, Z.; Busch, H.; Klein, F.; Grabowy, U.; Kopnarski, M. Enhanced ionization sputtering: A concept for superior industrial coatings. *Surf. Coat. Technol.* **2014**, *255*, 43–51. [[CrossRef](#)]
74. Helmersson, U.; Lattemann, M.; Bohlmark, J.; Ehiasarian, A.P.; Gudmundsson, J.T. Ionized physical vapor deposition (IPVD): A review of technology and applications. *Thin Solid Films* **2006**, *513*, 1–24. [[CrossRef](#)]
75. Bobzin, K.; Brögelmann, T.; Kalscheuer, C. Arc PVD (Cr,Al,Mo)N and (Cr,Al,Cu)N coatings for mobility applications. *Surf. Coat. Technol.* **2020**, *384*, 125046. [[CrossRef](#)]
76. Li, H.; Li, D.; Wang, Z.; Li, Y.; Zhang, X.; Wang, S.; Liu, X. Effects of trace La addition on corrosion properties of oxygen-free copper tube in a formic acid environment. *Mater. Corros.* **2023**, *74*, 1058–1065. [[CrossRef](#)]
77. Ko, J.; Kim, J.W.; Min, H.W.; Kim, Y.; Yoon, Y.S. Review of manufacturing technologies for coated accident tolerant fuel cladding. *J. Nucl. Mater.* **2022**, *561*, 153562. [[CrossRef](#)]
78. Tarek, A.H.J.; Lai, C.W.; Abd Razak, B.; Wong, Y.H. Physical Vapour Deposition of Zr-Based Nano Films on Various Substrates: A Review. *Curr. Nanosci.* **2022**, *18*, 347–366. [[CrossRef](#)]
79. Ye, Q.W.; Li, Y.; Zhang, M.Y.; Zhang, S.Z.; Bi, Y.J.; Gao, X.P.; He, Y.Y. Electrochemical behavior of (Cr, W, Al, Ti, Si)N multilayer coating on nitrated AISI 316L steel in natural seawater. *Ceram. Int.* **2020**, *46*, 22404–22418. [[CrossRef](#)]
80. Bello, M.; Shanmugan, S. Achievements in mid and high-temperature selective absorber coatings by physical vapor deposition (PVD) for solar thermal Application—A review. *J. Alloys Compd.* **2020**, *839*, 155510. [[CrossRef](#)]
81. Bootkul, D.; Saenphinit, N.; Supsermpol, B.; Aramwit, C.; Intarasiri, S. Synthesis of Ti-doped DLC film on SS304 steels by Filtered Cathodic Vacuum Arc (FCVA) technique for tribological improvement. *Appl. Surf. Sci.* **2014**, *310*, 293–299. [[CrossRef](#)]
82. Shen, Y.; Luo, J.; Liao, B.; Chen, L.; Zhang, X.; Zhao, Y.; Pang, P.; Zeng, X. Enhanced Anti-Tribocorrosion Performance of Ti-DLC Coatings Deposited by Filtered Cathodic Vacuum Arc with the Optimization of Bias Voltage. *Coatings* **2022**, *12*, 697. [[CrossRef](#)]
83. Chen, X.; Peng, Z.; Yu, X.; Fu, Z.; Yue, W.; Wang, C. Microstructure and tribological performance of self-lubricating diamond/tetrahedral amorphous carbon composite film. *Appl. Surf. Sci.* **2011**, *257*, 3180–3186. [[CrossRef](#)]
84. Shen, Y.; Luo, J.; Liao, B.; Zhang, X.; Zhao, Y.; Zeng, X.; Chen, L.; Pang, P.; Bao, F. Tribocorrosion and tribological behavior of Ti-DLC coatings deposited by filtered cathodic vacuum arc. *Diam. Relat. Mater.* **2022**, *125*, 108985. [[CrossRef](#)]
85. Barranco, A.; Borrás, A.; Gonzalez-Elipe, A.R.; Palmero, A. Perspectives on oblique angle deposition of thin films: From fundamentals to devices. *Prog. Mater. Sci.* **2016**, *76*, 59–153. [[CrossRef](#)]
86. Kuo, C.C.; Liu, C.C.; Lin, C.C.; Liou, Y.Y.; Lan, Y.F.; He, J.L. Effects of oxygen flow rate on microstructure and properties of indium molybdenum oxide films by ion beam-assisted deposition. *Vacuum* **2008**, *82*, 441–447. [[CrossRef](#)]
87. Martinu, L.; Zabeida, O.; Klemberg-Sapieha, J.E. Chapter 9—Plasma-Enhanced Chemical Vapor Deposition of Functional Coatings. In *Handbook of Deposition Technologies for Films and Coatings*, 3rd ed.; Martin, P.M., Ed.; William Andrew Publishing: Boston, MA, USA, 2010; pp. 392–465.
88. Sahoo, S.; Sahoo, G.; Jeong, S.M.; Rout, C.S. A review on supercapacitors based on plasma enhanced chemical vapor deposited vertical graphene arrays. *J. Energy Storag.* **2022**, *53*, 105212. [[CrossRef](#)]
89. Li, Y.; Wang, Z.; Shao, M.; Zhang, Z.; Wang, C.; Yan, J.; Lu, J.; Zhang, L.; Xie, B.; He, Y.; et al. Characterization and electrochemical behavior of a multilayer-structured Ti-N layer produced by plasma nitriding of electron beam melting TC4 alloy in Hank's solution. *Vacuum* **2023**, *208*, 111737. [[CrossRef](#)]
90. Chang, S.-H.; Tang, T.-C.; Huang, K.-T.; Liu, C.-M. Investigation of the characteristics of DLC films on oxynitriding-treated ASP23 high speed steel by DC-pulsed PECVD process. *Surf. Coat. Technol.* **2015**, *261*, 331–336. [[CrossRef](#)]
91. Muthuraja, A.; Naik, S.; Rajak, D.K.; Pruncu, C.I. Experimental investigation on chromium-diamond like carbon (Cr-DLC) coating through plasma enhanced chemical vapour deposition (PECVD) on the nozzle needle surface. *Diam. Relat. Mater.* **2019**, *100*, 107588. [[CrossRef](#)]
92. Ensinger, W. Correlations between process parameters and film properties of diamond-like carbon films formed by hydrocarbon plasma immersion ion implantation. *Surf. Coat. Technol.* **2009**, *203*, 2721–2726. [[CrossRef](#)]

93. Lu, T.; Qiao, Y.Q.; Liu, X.Y. Surface modification of biomaterials using plasma immersion ion implantation and deposition. *Interface Focus* **2012**, *2*, 325–336. [[CrossRef](#)]
94. Liu, K.; Wang, X.; Liu, J.; Hu, Y.; Zhong, H.; Pan, Q.; Luo, L.; Chen, S.; Zhang, Y.; Long, Z. Nitride layers on uranium surfaces. *Prog. Surf. Sci.* **2018**, *93*, 47–84. [[CrossRef](#)]
95. Vincent, S.; Bot, C.L.; Sarret, F.; Meillot, E.; Caltagirone, J.-P.; Bianchi, L. Penalty and Eulerian–Lagrangian VOF methods for impact and solidification of metal droplets plasma spray process. *Comput. Fluids* **2015**, *113*, 32–41. [[CrossRef](#)]
96. Das, R.; Bandyopadhyay, P.P. Processing of solid lubricant doped ceramic powder feedstock using heterocoagulation technique for plasma spraying. *Ceram. Int.* **2022**, *48*, 25592–25609. [[CrossRef](#)]
97. Zhao, X.Q.; An, Y.L.; Hou, G.L.; Zhou, H.D.; Chen, J.M. Friction and Wear Behavior of Plasma-Sprayed Al₂O₃-13 wt.%TiO₂ Coatings Under the Lubrication of Liquid Paraffin. *J. Therm. Spray Technol.* **2014**, *23*, 666–675. [[CrossRef](#)]
98. Gautam, R.K.S.; Rao, U.S.; Tyagi, R. High temperature tribological properties of Ni-based self-lubricating coatings deposited by atmospheric plasma spray. *Surf. Coat. Technol.* **2019**, *372*, 390–398. [[CrossRef](#)]
99. Feng, C.; Mcenaney, K.; Gang, C.; Ren, Z. A review of cermet-based spectrally selective solar absorbers. *Energy Environ. Sci.* **2014**, *7*, 1615–1627.
100. Vautherin, B.; Planche, M.P.; Bolot, R.; Quet, A.; Bianchi, L.; Montavon, G. Vapors and Droplets Mixture Deposition of Metallic Coatings by Very Low Pressure Plasma Spraying. *J. Therm. Spray Technol.* **2014**, *23*, 596–608. [[CrossRef](#)]
101. Liu, S.H.; Trelles, J.P.; Murphy, A.B.; He, W.T.; Guo, H.B. Low-Pressure Plasma-Induced Physical Vapor Deposition of Advanced Thermal Barrier Coatings: Microstructures, Modelling and Mechanisms. *Mater. Today Phys.* **2021**, *21*, 100481. [[CrossRef](#)]
102. Akpek, A. Analysis of Surface Properties of Ag and Ti Ion-Treated Medical Textiles by Metal Vapor Vacuum Arc Ion Implantation. *Coatings* **2021**, *11*, 102. [[CrossRef](#)]
103. Aliofkhaezrai, M.; Macdonald, D.D.; Matykina, E.; Parfenov, E.V.; Egorkin, V.S.; Curran, J.A.; Troughton, S.C.; Sinebryukhov, S.L.; Gnedenkov, S.V.; Lampke, T.; et al. Review of plasma electrolytic oxidation of titanium substrates: Mechanism, properties, applications and limitations. *Appl. Surf. Sci. Adv.* **2021**, *5*, 100121. [[CrossRef](#)]
104. Molaei, M.; Babaei, K.; Fattah-alhosseini, A. Improving the wear resistance of plasma electrolytic oxidation (PEO) coatings applied on Mg and its alloys under the addition of nano- and micro-sized additives into the electrolytes: A review. *J. Magnes. Alloys* **2021**, *9*, 1164–1186. [[CrossRef](#)]
105. Fattah-alhosseini, A.; Chaharmahali, R.; Keshavarz, M.K.; Babaei, K. Surface characterization of bioceramic coatings on Zr and its alloys using plasma electrolytic oxidation (PEO): A review. *Surf. Interfaces* **2021**, *25*, 101283. [[CrossRef](#)]
106. Huang, Y.; Sun, X.; Song, J.; Chen, J.; Gao, J.; Xiao, K. Study on corrosion protection behavior of magnesium alloy/micro-arc oxidation coating in neutral salt spray environment. *Int. J. Electrochem. Sci.* **2023**, *18*, 100179. [[CrossRef](#)]
107. Ding, Z.-Y.; Wang, Y.-H.; Ouyang, J.-H.; Liu, Z.-G.; Wang, Y.-M.; Wang, Y.-J. Influence of Al₂O₃ addition in NaAlO₂ electrolyte on microstructure and high-temperature properties of plasma electrolytic oxidation ceramic coatings on Ti₂AlNb alloy. *Surf. Coat. Technol.* **2019**, *370*, 187–195. [[CrossRef](#)]
108. Grundsteins, K.; Diedkova, K.; Korniienko, V.; Stoppel, A.; Balakin, S.; Jekabsons, K.; Riekstina, U.; Waloszczyk, N.; Kołkowska, A.; Varava, Y.; et al. Nanodiamond Decorated PEO Oxide Coatings on NiTi Alloy. *Nanomaterials* **2023**, *13*, 2601. [[CrossRef](#)] [[PubMed](#)]
109. Li, G.; Ma, F.; Liu, P.; Qi, S.; Li, W.; Zhang, K.; Chen, X. Review of micro-arc oxidation of titanium alloys: Mechanism, properties and applications. *J. Alloys Compd.* **2023**, *948*, 169773. [[CrossRef](#)]
110. Qin, Y.K.; Xiong, D.S.; Li, J.L. Tribological properties of laser surface textured and plasma electrolytic oxidation duplex-treated Ti6Al4V alloy deposited with MoS₂ film. *Surf. Coat. Technol.* **2015**, *269*, 266–272. [[CrossRef](#)]
111. Qin, Y.K.; Xiong, D.S.; Li, J.L. Characterization and friction behavior of LST/PEO duplex-treated Ti6Al4V alloy with burnished MoS₂ film. *Appl. Surf. Sci.* **2015**, *347*, 475–484. [[CrossRef](#)]
112. Rocca, E.; Veys-Renaux, D.; Guessoum, K. Electrochemical behavior of zinc in KOH media at high voltage: Micro-arc oxidation of zinc. *J. Electroanal. Chem.* **2015**, *754*, 125–132. [[CrossRef](#)]
113. Tran, Q.-P.; Kuo, Y.-C.; Sun, J.-K.; He, J.-L.; Chin, T.-S. High quality oxide-layers on Al-alloy by micro-arc oxidation using hybrid voltages. *Surf. Coat. Technol.* **2016**, *303*, 61–67. [[CrossRef](#)]
114. Zhang, X.; Yang, L.; Lu, X.; Lv, Y.; Jiang, D.; Yu, Y.; Peng, Z.; Dong, Z. Characterization and property of dual-functional Zn-incorporated TiO₂ micro-arc oxidation coatings: The influence of current density. *J. Alloys Compd.* **2019**, *810*, 151893. [[CrossRef](#)]
115. Bai, L.; Dong, B.; Chen, G.; Xin, T.; Wu, J.; Sun, X. Effect of positive pulse voltage on color value and corrosion property of magnesium alloy black micro-arc oxidation ceramic coating. *Surf. Coat. Technol.* **2019**, *374*, 402–408. [[CrossRef](#)]
116. Chai, Y.; Yan, J.; Wang, C.; Mei, L. Effect of electrical parameters on the growth and properties of 7075 aluminum alloy film based on scanning micro-arc oxidation with mesh electrode. *J. Mater. Res. Technol.* **2023**, *25*, 988–998. [[CrossRef](#)]
117. Farshid, S.; Kharaziha, M. Micro and nano-enabled approaches to improve the performance of plasma electrolytic oxidation coated magnesium alloys. *J. Magnes. Alloys* **2021**, *9*, 1487–1504. [[CrossRef](#)]
118. Kaseem, M.; Fatimah, S.; Nashrah, N.; Ko, Y.G. Recent progress in surface modification of metals coated by plasma electrolytic oxidation: Principle, structure, and performance. *Prog. Mater. Sci.* **2021**, *117*, 100735. [[CrossRef](#)]
119. Wang, L.S.; Bu, Z.X.; Lu, M.; Geng, Y.; Chen, M.H.; Sun, L. Thick oxide coatings formed by spark anodizing of Mg-Al alloy in alkaline phosphate-silicate electrolytes. *J. Alloys Compd.* **2017**, *710*, 121–129. [[CrossRef](#)]

120. Kamal Jayaraj, R.; Malarvizhi, S.; Balasubramanian, V. Optimizing the micro-arc oxidation (MAO) parameters to attain coatings with minimum porosity and maximum hardness on the friction stir welded AA6061 aluminium alloy welds. *Def. Technol.* **2017**, *13*, 111–117. [[CrossRef](#)]
121. Zhang, G.; Huang, S.; Li, X.; Zhao, D.; Cao, Y.; Liu, B.; Huang, Q. Oxide ceramic coatings with amorphous/nano-crystalline dual-structures prepared by micro-arc oxidation on Ti-Nb-Zr medium entropy alloy surfaces for biomedical applications. *Ceram. Int.* **2023**, *49*, 18114–18124. [[CrossRef](#)]
122. Babaei, K.; Fattah-alhosseini, A.; Molaei, M. The effects of carbon-based additives on corrosion and wear properties of Plasma electrolytic oxidation (PEO) coatings applied on Aluminum and its alloys: A review. *Surf. Interfaces* **2020**, *21*, 100677. [[CrossRef](#)]
123. Chen, W.; Yu, Y.; Tieu, A.K.; Hao, J.; Wang, L.; Zhu, S.; Yang, J. Microstructure, mechanical properties and tribological behavior of the low-pressure cold sprayed tin bronze-alumina coating in artificial seawater. *Tribol. Int.* **2020**, *142*, 105992. [[CrossRef](#)]
124. Xiao, J.-K.; Zhang, W.; Liu, L.-M.; Gan, X.-P.; Zhou, K.-C.; Zhang, C. Microstructure and tribological properties of plasma sprayed Cu-15Ni-8Sn coatings. *Surf. Coat. Technol.* **2018**, *337*, 159–167. [[CrossRef](#)]
125. Fernandes, F.; AL-Rjoub, A.; Cavaleiro, D.; Polcar, T.; Cavaleiro, A. Room and High Temperature Tribological Performance of Multilayered TiSiN/TiN and TiSiN/TiN(Ag) Coatings Deposited by Sputtering. *Coatings* **2020**, *10*, 1191. [[CrossRef](#)]
126. Ju, H.; Huang, K.; Luan, J.; Geng, Y.; Yang, J.; Xu, J. Evaluation under temperature cycling of the tribological properties of Ag-SiN_x films for green tribological applications. *Ceram. Int.* **2023**, *49*, 30115–30124. [[CrossRef](#)]
127. Liu, X.G.; Jamvasant, C.; Liu, C.; Matthews, A.; Leyland, A. CrCuAgN PVD nanocomposite coatings: Effects of annealing on coating morphology and nanostructure. *Appl. Surf. Sci.* **2017**, *392*, 732–746. [[CrossRef](#)]
128. Vidiš, M.; Truchlý, M.; Izai, V.; Fiantok, T.; Rajnec, M.; Roch, T.; Satrapinskyy, L.; Haršáni, M.; Nagy, Š.; Turiničová, V.; et al. Mechanical and Tribological Properties of Ag/TiB_x Nanocomposite Thin Films with Strong Antibacterial Effect Prepared by Magnetron Co-Sputtering. *Coatings* **2023**, *13*, 989. [[CrossRef](#)]
129. Ye, F.; Lou, Z.; Wang, Y.; Liu, W. Wear mechanism of Ag as solid lubricant for wide range temperature application in micro-beam plasma cladded Ni60 coatings. *Tribol. Int.* **2022**, *167*, 107402. [[CrossRef](#)]
130. Mu, Y.T.; Liu, M.; Wang, Y.X.; Liu, E.Y. PVD multilayer VN-VN/Ag composite coating with adaptive lubricious behavior from 25 to 700 °C. *Rsc Adv.* **2016**, *6*, 53043–53053. [[CrossRef](#)]
131. de Castilho, B.; Munagala, V.N.V.; Alidokht, S.A.; Sharifi, N.; Bessette, S.; Makowiec, M.E.; Gauvin, R.; Stoyanov, P.; Moreau, C.; Chromik, R.R. Insights on Silver Migration Mechanisms and their Influence on the Wear Behavior of Thermally Sprayed Self-lubricating Coatings Up to 350 °C. *Tribol. Lett.* **2022**, *70*, 120. [[CrossRef](#)]
132. Akhtar, S.S. A critical review on self-lubricating ceramic-composite cutting tools. *Ceram. Int.* **2021**, *47*, 20745–20767. [[CrossRef](#)]
133. Magnéli, A. Structures of the ReO₃-type with recurrent dislocations of atoms: ‘Homologous series’ of molybdenum and tungsten oxides. *Acta Crystallogr.* **1953**, *6*, 495–500. [[CrossRef](#)]
134. Erdemir, A. A crystal chemical approach to the formulation of self-lubricating nanocomposite coatings. *Surf. Coat. Technol.* **2005**, *200*, 1792–1796. [[CrossRef](#)]
135. Franz, R.; Mitterer, C. Vanadium containing self-adaptive low-friction hard coatings for high-temperature applications: A review. *Surf. Coat. Technol.* **2013**, *228*, 1–13. [[CrossRef](#)]
136. Najafi, H.; Karimi, A.; Dessarzin, P.; Morstein, M. Correlation between anionic substitution and structural properties in AlCr(OxN_{1-x}) coatings deposited by lateral rotating cathode arc PVD. *Thin Solid Films* **2011**, *520*, 1597–1602. [[CrossRef](#)]
137. Gulbiński, W.; Suszko, T.; Sienicki, W.; Warcholiński, B. Tribological properties of silver- and copper-doped transition metal oxide coatings. *Wear* **2003**, *254*, 129–135. [[CrossRef](#)]
138. Ouyang, J.H.; Sasaki, S.; Umeda, K. The friction and wear characteristics of low-pressure plasma-sprayed ZrO₂-BaCrO₄ composite coating at elevated temperatures. *Surf. Coat. Technol.* **2002**, *154*, 131–139. [[CrossRef](#)]
139. Yin, B.; Peng, Z.; Liang, J.; Jin, K.; Zhu, S.; Yang, J.; Qiao, Z. Tribological behavior and mechanism of self-lubricating wear-resistant composite coatings fabricated by one-step plasma electrolytic oxidation. *Tribol. Int.* **2016**, *97*, 97–107. [[CrossRef](#)]
140. Wang, Y.M.; Jiang, B.L.; Guo, L.X.; Lei, T.Q. Tribological behavior of microarc oxidation coatings formed on titanium alloys against steel in dry and solid lubrication sliding. *Appl. Surf. Sci.* **2006**, *252*, 2989–2998. [[CrossRef](#)]
141. Zhang, J.-M.; Xin, H.; Wei, X.-M. Atomic-scale calculation of interface energy for Ag/Ni. *Appl. Surf. Sci.* **2005**, *246*, 14–22. [[CrossRef](#)]
142. Tuo, Y.; Yang, Z.; Guo, Z.; Chen, Y.; Hao, J.; Zhao, Q.; Kang, Y.; Zhang, Y.; Zhao, Y. Pore structure optimization of MoS₂/Al₂O₃ self-lubricating ceramic coating for improving corrosion resistance. *Vacuum* **2023**, *207*, 111687. [[CrossRef](#)]
143. Satish, C.; Vijay Kumar, K.; Prasad, S.; Sai Kiran, P.; Asiq Rahman, O.S.; Singh, P.; Indupuri, S.; Shrivastava, R.; Pandey, S.M.; Keshri, A.K. Effect of Al₂O₃ and MoS₂ reinforcement on microstructure, mechanical, and wear properties of plasma sprayed aluminium hybrid composite coating. *Mater. Today Commun.* **2023**, *36*, 106640. [[CrossRef](#)]
144. Kim, S.-H.; Jeong, S.-H.; Kim, T.-H.; Choi, J.-H.; Cho, S.-H.; Kim, B.S.; Lee, S.W. Effects of solid lubricant and laser surface texturing on tribological behaviors of atmospheric plasma sprayed Al₂O₃-ZrO₂ composite coatings. *Ceram. Int.* **2017**, *43*, 9200–9206. [[CrossRef](#)]
145. Żórawski, W.; Chatys, R.; Radek, N.; Borowiecka-Jamrozek, J. Plasma-sprayed composite coatings with reduced friction coefficient. *Surf. Coat. Technol.* **2008**, *202*, 4578–4582. [[CrossRef](#)]

146. Verma, R.; Sharma, S.; Mukherjee, B.; Singh, P.; Islam, A.; Keshri, A.K. Microstructural, mechanical and marine water tribological properties of plasma-sprayed graphene nanoplatelets reinforced Al₂O₃- 40 wt% TiO₂ coating. *J. Eur. Ceram. Soc.* **2022**, *42*, 2892–2904. [[CrossRef](#)]
147. Wang, Y.; Wan, W.; Mao, J.; Tian, L.; Li, R. Microstructure and Wear Behavior of Plasma-Sprayed TiO₂-SiAlON Ceramic Coating. *Coatings* **2020**, *10*, 1268. [[CrossRef](#)]
148. Barati, N.; Meletis, E.L.; Golestani Fard, F.; Yerokhin, A.; Rastegari, S.; Faghihi-Sani, M.A. Al₂O₃-ZrO₂ nanostructured coatings using DC plasma electrolytic oxidation to improve tribological properties of Al substrates. *Appl. Surf. Sci.* **2015**, *356*, 927–934. [[CrossRef](#)]
149. Chen, J.-X.; Yang, Y.; Etim, I.P.; Tan, L.-L.; Yang, K.; Misra, R.D.K.; Wang, J.-H.; Su, X.-P. In vitro degradation, wear property and biocompatibility of nano-Y₂O₃-containing micro-arc oxidation coating on ZK60 alloy. *Trans. Nonferrous Met. Soc. China* **2023**, *33*, 1411–1424. [[CrossRef](#)]
150. Ouyang, J.-H.; Liang, X.-S.; Liu, Z.-G.; Yang, Z.-L.; Wang, Y.-J. Friction and wear properties of hot-pressed NiCr-BaCr₂O₄ high temperature self-lubricating composites. *Wear* **2013**, *301*, 820–827. [[CrossRef](#)]
151. Yang, H.; Wu, X.; Du, S.; Wang, C.; Guo, F.; Lu, H. Synergistic effect of “double pores” texture on tribological properties of AZ31 Mg alloy micro-arc oxide ceramic coatings. *Surf. Coat. Technol.* **2023**, *470*, 129875. [[CrossRef](#)]
152. Stone, D.S.; Harbin, S.; Mohseni, H.; Mogonye, J.E.; Scharf, T.W.; Muratore, C.; Voevodin, A.A.; Martini, A.; Aouadi, S.M. Lubricious silver tantalate films for extreme temperature applications. *Surf. Coat. Technol.* **2013**, *217*, 140–146. [[CrossRef](#)]
153. Mei, H.; Ding, J.C.; Yan, K.; Peng, W.; Zhao, C.; Luo, Q.; Gong, W.; Ren, F.; Wang, Q. Effects of V and Cu codoping on the tribological properties and oxidation behavior of AlTiN coatings. *Ceram. Int.* **2022**, *48*, 22276–22286. [[CrossRef](#)]
154. Fu, X.J.; Li, Y.; Su, H.J.; Cao, L.; Wan, Y.; Li, R.C. Tribological interactions between TiN PVD coating and MoDTC under boundary lubrication conditions. *Vacuum* **2022**, *195*, 110646. [[CrossRef](#)]
155. Kivak, T.; Sarikaya, M.; Yildirim, C.V.; Sirin, S. Study on turning performance of PVD TiN coated Al₂O₃+TiCN ceramic tool under cutting fluid reinforced by nano-sized solid particles. *J. Manuf. Process.* **2020**, *56*, 522–539. [[CrossRef](#)]
156. Wang, Y.F.; Li, Y.J.; Wu, G.Z.; Lu, Z.B. Friction reduction mechanisms of TiN film sliding in graphene aqueous dispersion. *Lubr. Sci.* **2022**, *34*, 112–126. [[CrossRef](#)]
157. Esteve, J.; Martínez, E.; Lousa, A.; Montalà, F.; Carreras, L.L. Microtribological characterization of group V and VI metal-carbide wear-resistant coatings effective in the metal casting industry. *Surf. Coat. Technol.* **2000**, *133–134*, 314–318. [[CrossRef](#)]
158. Zhang, L.; Shao, M.; Wang, Z.; Zhang, Z.; He, Y.; Yan, J.; Lu, J.; Qiu, J.; Li, Y. Comparison of tribological properties of nitrided Ti-N modified layer and deposited TiN coatings on TA2 pure titanium. *Tribol. Int.* **2022**, *174*, 107712. [[CrossRef](#)]
159. Li, Y.; Liu, Z.L.; Luo, J.B.; Zhang, S.Z.; Qiu, J.X.; He, Y.Y. Microstructure, mechanical and adhesive properties of CrN/CrTiAlSiN/WCrTiAlN multilayer coatings deposited on nitrided AISI 4140 steel. *Mater. Charact.* **2019**, *147*, 353–364. [[CrossRef](#)]
160. Li, Y.; Ye, Q.W.; Zhu, Y.J.; Zhang, L.; He, Y.Y.; Zhang, S.Z.; Xiu, J.J. Microstructure, adhesion and tribological properties of CrN/CrTiAlSiN/WCrTiAlN multilayer coatings deposited on nitrocarburized AISI 4140 steel. *Surf. Coat. Technol.* **2019**, *362*, 27–34. [[CrossRef](#)]
161. Ju, H.; Zhou, R.; Liu, S.; Yu, L.; Xu, J.; Geng, Y. Enhancement of the tribological behavior of self-lubricating nanocomposite Mo₂N/Cu films by adding the amorphous SiNx. *Surf. Coat. Technol.* **2021**, *423*, 127565. [[CrossRef](#)]
162. Tang, J.-F.; Lin, C.-Y.; Yang, F.-C.; Chang, C.-L. Influence of Nitrogen Content and Bias Voltage on Residual Stress and the Tribological and Mechanical Properties of CrAlN Films. *Coatings* **2020**, *10*, 546. [[CrossRef](#)]
163. Hudec, T.; Izai, V.; Satrapinskyy, L.; Huminiuc, T.; Roch, T.; Gregor, M.; Grančič, B.; Mikula, M.; Polcar, T. Structure, mechanical and tribological properties of MoSe₂ and Mo-Se-N solid lubricant coatings. *Surf. Coat. Technol.* **2021**, *405*, 126536. [[CrossRef](#)]
164. Bobzin, K.; Brögelmann, T.; Kalscheuer, C.; Thiex, M. Self-lubricating triboactive (Cr,Al)N plus Mo:S coatings for fluid-free applications. *J. Mater. Sci.* **2021**, *56*, 15040–15060. [[CrossRef](#)]
165. Xu, X.; Su, F.H.; Li, Z.J. Tribological properties of nanostructured TiAlN/W₂N multilayer coating produced by PVD. *Wear* **2019**, *430*, 73–81. [[CrossRef](#)]
166. Zhang, J.; Su, X.; Shan, L.; Liu, Y.; Zhang, P.; Jia, Y. Preparation and tribocorrosion performance of CrCN coatings in artificial seawater on different substrates with different bias voltages. *Ceram. Int.* **2019**, *45*, 9901–9911. [[CrossRef](#)]
167. Wang, Q.; Zhou, F.; Callisti, M.; Polcar, T.; Kong, J.; Yan, J. Study on the crack resistance of CrBN composite coatings via nano-indentation and scratch tests. *J. Alloys Compd.* **2017**, *708*, 1103–1109. [[CrossRef](#)]
168. Wang, Q.; Wu, Z.; Zhou, F.; Huang, H.; Niitsu, K.; Yan, J.J.S.; Technology, C. Evaluation of crack resistance of CrSiCN coatings as a function of Si concentration via nanoindentation. *Surf. Coat. Technol.* **2015**, *272*, 239–245. [[CrossRef](#)]
169. Wo, P.C.; Munroe, P.R.; Jiang, Z.T.; Zhou, Z.; Li, K.Y.; Xie, Z. Enhancing toughness of CrN coatings by Ni addition for safety-critical applications. *Mater. Sci. Eng. A* **2014**, *596*, 264–274. [[CrossRef](#)]
170. Huang, B.; Zhou, Q.; An, Q.; Zhang, E.G.; Chen, Q.; Liang, D.D.; Du, H.M.; Li, Z.M. Tribological performance of the gradient composite TiAlSiN coating with various friction pairs. *Surf. Coat. Technol.* **2022**, *429*, 127945. [[CrossRef](#)]
171. Cheng, C.; Li, H.; Zhang, C.; Guo, C.; Li, J.; Zhang, H.; Lin, S.; Wang, Q. Effect of substrate bias on structure and properties of (AlTiCrZrNb)N high-entropy alloy nitride coatings through arc ion plating. *Surf. Coat. Technol.* **2023**, *467*, 129692. [[CrossRef](#)]
172. Li, Y.; Wang, Z.W.; Zhang, Z.H.; Shao, M.H.; Lu, J.P.; Yan, J.W.; Zhang, L.; He, Y.Y. Microstructure and tribological properties of multilayered ZrCrW(C)N coatings fabricated by cathodic vacuum-arc deposition. *Ceram. Int.* **2022**, *48*, 36655–36669. [[CrossRef](#)]

173. Wang, Z.W.; Li, Y.; Zhang, Z.H.; Zhang, S.Z.; Ren, P.; Qiu, J.X.; Wang, W.W.; Bi, Y.J.; He, Y.Y. Friction and wear behavior of duplex-treated AISI 316L steels by rapid plasma nitriding and (CrWAlTiSi)N ceramic coating. *Results Phys.* **2021**, *24*, 104132. [[CrossRef](#)]
174. Bobzin, K.; Kalscheuer, C.; Möbius, M.P.; Rank, M.; Oehler, M.; Koch, O. Triboactive coatings for wear and friction reduction in chain drives. *Tribol. Int.* **2023**, *185*, 108562. [[CrossRef](#)]
175. Polcar, T.; Martinez, R.; Vitù, T.; Kopecký, L.; Rodriguez, R.; Cavaleiro, A. High temperature tribology of CrN and multilayered Cr/CrN coatings. *Surf. Coat. Technol.* **2009**, *203*, 3254–3259. [[CrossRef](#)]
176. Jasempoor, F.; Elmkhah, H.; Imantalab, O.; Fattah-alhosseini, A. Improving the mechanical, tribological, and electrochemical behavior of AISI 304 stainless steel by applying CrN single layer and Cr/CrN multilayer coatings. *Wear* **2022**, *504–505*, 204425. [[CrossRef](#)]
177. Wang, Y.; Zhang, J.; Wang, Y.; Wang, C.; Guo, W.; Lu, X.; Sui, Y.; Lan, J. Inhibiting tribocorrosion damage of Cr/CrxN coatings by multi-layer design. *Ceram. Int.* **2021**, *47*, 842–850. [[CrossRef](#)]
178. Wang, T.-C.; Hsu, S.-Y.; Lai, Y.-T.; Tsai, S.-Y.; Duh, J.-G. Microstructure and high-temperature tribological characteristics of self-lubricating TiAlSiN/VSiN multilayer nitride coatings. *Mater. Chem. Phys.* **2023**, *295*, 127149. [[CrossRef](#)]
179. Dang, C.; Li, J.; Wang, Y.; Chen, J. Structure, mechanical and tribological properties of self-toughening TiSiN/Ag multilayer coatings on Ti6Al4V prepared by arc ion plating. *Appl. Surf. Sci.* **2016**, *386*, 224–233. [[CrossRef](#)]
180. Fu, Y.-D.; Zhu, X.-S.; Li, Z.-F.; Leng, K. Properties and microstructure of Ti6Al4V by deformation accelerated low temperature plasma nitriding. *Trans. Nonferrous Met. Soc. China* **2016**, *26*, 2609–2616. [[CrossRef](#)]
181. Samanta, A.; Bhattacharya, M.; Ratha, I.; Chakraborty, H.; Datta, S.; Ghosh, J.; Bysakh, S.; Sreemany, M.; Rane, R.; Joseph, A.; et al. Nano- and micro-tribological behaviours of plasma nitrided Ti6Al4V alloys. *J. Mech. Behav. Biomed. Mater.* **2018**, *77*, 267–294. [[CrossRef](#)]
182. Feng, W.; Yan, D.; He, J.; Li, X.; Dong, Y. Reactive plasma sprayed TiN coating and its tribological properties. *Wear* **2005**, *258*, 806–811. [[CrossRef](#)]
183. Proudhon, H.; Savkova, J.; Basseville, S.; Guipont, V.; Jeandin, M.; Cailletaud, G. Experimental and numerical wear studies of porous Reactive Plasma Sprayed Ti–6Al–4V/TiN composite coating. *Wear* **2014**, *311*, 159–166. [[CrossRef](#)]
184. Rodríguez, R.J.; García, J.A.; Medrano, A.; Rico, M.; Sánchez, R.; Martínez, R.; Labrugère, C.; Lahaye, M.; Guette, A. Tribological behaviour of hard coatings deposited by arc-evaporation PVD. *Vacuum* **2002**, *67*, 559–566. [[CrossRef](#)]
185. Zimmerman, J.H.; Guleryuz, C.G.; Krzanowski, J.E. Fabrication and tribological properties of titanium nitride coatings incorporating solid lubricant microreservoirs. *Surf. Coat. Technol.* **2008**, *202*, 2023–2032. [[CrossRef](#)]
186. Guleryuz, C.G.; Krzanowski, J.E. Mechanisms of self-lubrication in patterned TiN coatings containing solid lubricant microreservoirs. *Surf. Coat. Technol.* **2010**, *204*, 2392–2399. [[CrossRef](#)]
187. Tiron, V.; Velicu, I.-L.; Cristea, D.; Lupu, N.; Stoian, G.; Munteanu, D. Influence of ion-to-neutral flux ratio on the mechanical and tribological properties of TiN coatings deposited by HiPIMS. *Surf. Coat. Technol.* **2018**, *352*, 690–698. [[CrossRef](#)]
188. Cavaleiro, D.; Veeregowda, D.; Cavaleiro, A.; Carvalho, S.; Fernandes, F. High temperature tribological behaviour of TiSiN(Ag) films deposited by HiPIMS in DOMS mode. *Surf. Coat. Technol.* **2020**, *399*, 126176. [[CrossRef](#)]
189. Borgioli, F.; Galvanetto, E.; Galliano, F.P.; Bacci, T. Sliding wear resistance of reactive plasma sprayed Ti–TiN coatings. *Wear* **2006**, *260*, 832–837. [[CrossRef](#)]
190. Wu, S.; Zhao, Y.; Zhang, L.; Liu, S.; Qin, L.; Liao, B.; Zhang, X.; Chen, L.; Zhang, T. Effect of C doping on structure and properties of TiAlCrN coatings by filter cathode vacuum arc deposition. *Vacuum* **2022**, *201*, 111093. [[CrossRef](#)]
191. Tian, B.; Yue, W.; Fu, Z.; Gu, Y.; Wang, C.; Liu, J. Microstructure and tribological properties of W-implanted PVD TiN coatings on 316L stainless steel. *Vacuum* **2014**, *99*, 68–75. [[CrossRef](#)]
192. Yi, B.; Zhou, S.; Qiu, Z.; Zeng, D.C. The influences of pulsed bias duty cycle on tribological properties of solid lubricating TiMoCN coatings. *Vacuum* **2020**, *180*, 109552. [[CrossRef](#)]
193. Shtansky, D.V.; Sheveiko, A.N.; Petrzhik, M.I.; Kiryukhantsev-Korneev, F.V.; Levashov, E.A.; Leyland, A.; Yerokhin, A.L.; Matthews, A. Hard tribological Ti–B–N, Ti–Cr–B–N, Ti–Si–B–N and Ti–Al–Si–B–N coatings. *Surf. Coat. Technol.* **2005**, *200*, 208–212. [[CrossRef](#)]
194. Zhang, J.; Li, Z.; Wang, Y.; Zhou, S.; Wang, Y.; Zeng, Z.; Li, J. A new method to improve the tribological performance of metal nitride coating: A case study for CrN coating. *Vacuum* **2020**, *173*, 109158. [[CrossRef](#)]
195. Cheng, Y.H.; Browne, T.; Heckerman, B. Mechanical and tribological properties of CrN coatings deposited by large area filtered cathodic arc. *Wear* **2011**, *271*, 775–782. [[CrossRef](#)]
196. Mo, J.L.; Zhu, M.H. Tribological characterization of chromium nitride coating deposited by filtered cathodic vacuum arc. *Appl. Surf. Sci.* **2009**, *255*, 7627–7634. [[CrossRef](#)]
197. Zhang, L.; Shen, Y.-Q.; Zhao, Y.-M.; Chen, S.-N.; Ouyang, X.; Zhang, X.; Liang, H.; Liao, B.; Chen, L. Structure control of high-quality TiAlN Monolithic and TiAlN/TiAl multilayer coatings based on filtered cathodic vacuum arc technique. *Surf. Interfaces* **2023**, *38*, 102836. [[CrossRef](#)]
198. Soleimani, M.; Fattah-alhosseini, A.; Elmkhah, H.; Babaei, K.; Imantalab, O. A comparison of tribological and corrosion behavior of PVD-deposited CrN/CrAlN and CrCN/CrAlCN nanostructured coatings. *Ceram. Int.* **2023**, *49*, 5029–5041. [[CrossRef](#)]
199. Ren, Y.; Niu, Y.; Jia, J.; Cao, X.; Zhang, G. Design and tribological performance of CrN/Mo2N/MoSx composite coating in wide temperature range inspired by oxidation kinetics principle. *Tribol. Int.* **2023**, *180*, 108229. [[CrossRef](#)]

200. Lu, X.; Zhang, C.; Wang, C.; Cao, X.; Ma, R.; Sui, X.; Hao, J.; Liu, W. Investigation of (CrAlTiNbV)_{Nx} high-entropy nitride coatings via tailoring nitrogen flow rate for anti-wear applications in aviation lubricant. *Appl. Surf. Sci.* **2021**, *557*, 149813. [[CrossRef](#)]
201. Lu, X.; Zhang, C.; Zhang, X.; Cao, X.; Kang, J.; Sui, X.; Hao, J.; Liu, W. Dependence of mechanical and tribological performance on the microstructure of (CrAlTiNbV)_{Nx} high-entropy nitride coatings in aviation lubricant. *Ceram. Int.* **2021**, *47*, 27342–27350. [[CrossRef](#)]
202. Yang, Q. Wear resistance and solid lubricity of molybdenum-containing nitride coatings deposited by cathodic arc evaporation. *Surf. Coat. Technol.* **2017**, *332*, 283–295. [[CrossRef](#)]
203. Hudec, T.; Mikula, M.; Satrapinskyy, L.; Roch, T.; Truchlý, M.; Švec, P.; Huminiuc, T.; Polcar, T. Structure, mechanical and tribological properties of Mo-S-N solid lubricant coatings. *Appl. Surf. Sci.* **2019**, *486*, 1–14. [[CrossRef](#)]
204. Fenker, M.; Balzer, M.; Kellner, S.; Polcar, T.; Richter, A.; Schmidl, F.; Vitu, T. Formation of Solid Lubricants during High Temperature Tribology of Silver-Doped Molybdenum Nitride Coatings Deposited by dcMS and HIPIMS. *Coatings* **2021**, *11*, 1415. [[CrossRef](#)]
205. Gustavsson, F.; Jacobson, S.; Cavaleiro, A.; Polcar, T. Ultra-low friction W-S-N solid lubricant coating. *Surf. Coat. Technol.* **2013**, *232*, 541–548. [[CrossRef](#)]
206. Chetcuti, R.; Dearnley, P.A.; Mazzonello, A.; Buhagiar, J.; Mallia, B. Tribocorrosion response of duplex layered CoCrMoC/CrN and CrN/CoCrMoC coatings on implant grade 316LVM stainless steel. *Surf. Coat. Technol.* **2020**, *384*, 125313. [[CrossRef](#)]
207. Wang, J.; Han, B.; Chen, Z.; Wang, C.; Li, Y.; Neville, A.; Morina, A. Investigation on the Tribological Properties of FeS, Cu₂S, MoS₂, and WS₂ Sulfide Films Under Water Lubrication. *Tribol. Trans.* **2023**, *66*, 551–564. [[CrossRef](#)]
208. Piasecki, A.; Kotkowiak, M.; Tulinski, M.; Čep, R. Tribological Properties of Cu-MoS₂-WS₂-Ag-CNT Sintered Composite Materials. *Materials* **2022**, *15*, 8424. [[CrossRef](#)]
209. Bobzin, K.; Kalscheuer, C.; Thiex, M.; Stahl, K.; Lohner, T.; Maier, E.; Yilmaz, M. Adaptive (Cr, Al) N + Mo: S_g Coating for Highly-Stressed Contacts under Dry Rolling-Sliding Conditions. *Tribol. Int.* **2022**, *174*, 107761. [[CrossRef](#)]
210. Ba, D.; Sun, X.; Li, X.; Qiu, J.; Shi, Y.; Wang, Z. Effect of surface nanocrystallization layer on formation process of low temperature ion sulphurizing layer. *Integr. Ferroelectr.* **2017**, *182*, 21–29. [[CrossRef](#)]
211. Liu, Y.-D.; Wang, C.-B.; Yuan, J.-J.; Liu, J.-J. Investigation on anti-wear properties of sulfide layer on bearing steel lubricated by oil-containing FeS particles. *Surf. Coat. Technol.* **2010**, *205*, 470–474. [[CrossRef](#)]
212. Ma, G.-Z.; Xu, B.-S.; Wang, H.-D.; Si, H.-J. Effects of surface nanocrystallization pretreatment on low-temperature ion sulfurization behavior of 1Cr18Ni9Ti stainless steel. *Appl. Surf. Sci.* **2010**, *257*, 1204–1210. [[CrossRef](#)]
213. Zhuang, D.-M.; Liu, Y.-R.; Liu, J.-J.; Fang, X.-D.; Guang, M.-X.; Cui, Y. Microstructure and tribological properties of sulphide coating produced by ion sulphuration. *Wear* **1999**, *225–229*, 799–805. [[CrossRef](#)]
214. Peng, T.; Yan, Q.-Z.; Zhang, Y.; Shi, X.-J.; Ba, M.-Y. Low-cost solid FeS lubricant as a possible alternative to MoS₂ for producing Fe-based friction materials. *Int. J. Miner. Metall. Mater.* **2017**, *24*, 115–121. [[CrossRef](#)]
215. Wang, Q.; Li, X.; Niu, W.; Rui, X.; Mao, X.; Li, Y.; Yang, J. Effect of MoS₂ content on microstructure and properties of supersonic plasma sprayed Fe-based composite coatings. *Surf. Coat. Technol.* **2020**, *391*, 125699. [[CrossRef](#)]
216. Shi, S.S.; Wu, H.P.; Song, Y.T.; Handroos, H. Solid lubrication with MoS₂-Ti-C films for high-vacuum applications in a nuclear fusion experimental device. *Ind. Lubr. Tribol.* **2018**, *70*, 155–160. [[CrossRef](#)]
217. Yang, K.; Shi, X.L.; Zhai, W.Z. Effects of MoS₂ and Multiwalled Carbon Nanotubes on Tribological Behavior of TiAl Matrix Composite. *J. Mater. Eng. Perform.* **2016**, *25*, 1094–1102. [[CrossRef](#)]
218. Buck, V. Preparation and properties of different types of sputtered MoS₂ films. *Wear* **1987**, *114*, 263–274. [[CrossRef](#)]
219. Liu, W.; Wu, W.; Chhattal, M.; Zheng, Q.; Gao, X.; Ren, K.; Liu, G.; Geng, Z.; Gong, Z. Superlubricity of Titanium Alloy Enabled by MoS₂ Flakes and a-C:H Film. *Coatings* **2023**, *13*, 820. [[CrossRef](#)]
220. Ju, H.; Zhou, R.; Luan, J.; Yu, L.; Xu, J.; Zuo, B.; Yang, J.; Geng, Y.; Zhao, L.; Fernandes, F. Multilayer Mo₂N-Ag/SiN_x films for demanding applications: Morphology, structure and temperature-cycling tribological properties. *Mater. Des.* **2022**, *223*, 111128. [[CrossRef](#)]
221. Kokalj, D.; Debus, J.; Stangier, D.; Moldenhauer, H.; Nikolov, A.; Wittig, A.; Brümmer, A.; Tillmann, W. Controlling the Structural, Mechanical and Frictional Properties of MoS_x Coatings by High-Power Impulse Magnetron Sputtering. *Coatings* **2020**, *10*, 755. [[CrossRef](#)]
222. Seynstahl, A.; Krauß, S.; Bitzek, E.; Meyer, B.; Merle, B.; Tremmel, S. Microstructure, Mechanical Properties and Tribological Behavior of Magnetron-Sputtered MoS₂ Solid Lubricant Coatings Deposited under Industrial Conditions. *Coatings* **2021**, *11*, 455. [[CrossRef](#)]
223. Zhang, P.; Ying, P.; Lin, C.; Yang, T.; Wu, J.; Huang, M.; Wang, T.; Fang, Y.; Levchenko, V. Effect of Modulation Periods on the Mechanical and Tribological Performance of MoS₂-TiL/MoS₂-TiH Multilayer Coatings. *Coatings* **2021**, *11*, 1230. [[CrossRef](#)]
224. Fu, J.; Ma, D.; Fan, L.; Yu, Z.; Yin, H.; Ma, C. Tribological Properties of Solid Lubricant WS₂ in Dimples on the Cylinder of Diesel Engine at High Temperature. *Materials* **2022**, *15*, 8161. [[CrossRef](#)] [[PubMed](#)]
225. Hu, N.; Zhang, X.; Wang, X.; Wu, N.; Wang, S. Study on Tribological Properties and Mechanisms of Different Morphology WS₂ as Lubricant Additives. *Materials* **2020**, *13*, 1522. [[CrossRef](#)] [[PubMed](#)]
226. Yaqub, T.B.; Yaqoob, K.; Mukhtar, A.; Fernandes, F.; Bondarev, A.; Ferreira, F.; Al-Rjoub, A.; Cavaleiro, A. Vacuum Tribological Properties of W-S-N Coatings Synthesized by Direct Current Magnetron Sputtering. *Coatings* **2022**, *12*, 1646. [[CrossRef](#)]

227. Wang, H.-D.; Zhuang, D.-M.; Wang, K.-L.; Liu, J.-J. Comparison of the tribological properties of an ion sulfurized coating and a plasma sprayed FeS coating. *Mater. Sci. Eng. A* **2003**, *357*, 321–327.
228. Zhang, G.; Ma, Z.; Yin, Y.; Li, Q.; Li, C.; Ma, T.; Ma, S. Tribological performance analysis of nano-FeS films deposited on the surface of bearing steel. *Colloids Surf. A Physicochem. Eng. Asp.* **2023**, *671*, 131453. [[CrossRef](#)]
229. Mutyala, K.C.; Singh, H.; Fouts, J.A.; Evans, R.D.; Doll, G.L. Influence of MoS₂ on the Rolling Contact Performance of Bearing Steels in Boundary Lubrication: A Different Approach. *Tribol. Lett.* **2016**, *61*, 20. [[CrossRef](#)]
230. Feng, X.; Zhou, H.; Zheng, Y.; Zhang, K.; Zhang, Y. Tribological behavior and wear mechanism of Ti/MoS₂ films deposited on plasma nitrided CF170 steel sliding against different mating materials. *Vacuum* **2021**, *194*, 110623. [[CrossRef](#)]
231. Gao, K.; Wang, Y.; Zhang, B.; Zhang, J. Effect of vacuum atomic oxygen irradiation on the tribological properties of fullerene-like carbon and MoS₂ films. *Tribol. Int.* **2022**, *170*, 107499. [[CrossRef](#)]
232. Zeng, C.; Pu, J.; Wang, H.; Zheng, S.; Chen, R. Influence of microstructure on tribological properties and corrosion resistance of MoS₂/WS₂ films. *Ceram. Int.* **2020**, *46*, 13774–13783. [[CrossRef](#)]
233. Yue, W.; Sun, X.; Wang, C.; Fu, Z.; Liu, Y.; Liu, J. A comparative study on the tribological behaviors of nitrided and sulfur-nitrided 35CrMo steel lubricated in PAO base oil with MoDTC additive. *Tribol. Int.* **2011**, *44*, 2029–2034. [[CrossRef](#)]
234. Han, B.; Zhang, M.; Qi, C.; Cui, N.; Wang, Y. Characterization and friction-reduction performances of composite coating produced by laser cladding and ion sulfurizing. *Mater. Lett.* **2015**, *150*, 35–38. [[CrossRef](#)]
235. Yue, W.; Gao, X.; Liu, Y.; Sun, X.; Wang, C.; Liu, J. Tribological properties of sulfurized-nitrided layer prepared by a two-step method. *Vacuum* **2011**, *85*, 1011–1016. [[CrossRef](#)]
236. Wang, H.-D.; Xu, B.-S.; Liu, J.-J.; Zhuang, D.-M. Characterization and tribological properties of plasma sprayed FeS solid lubrication coatings. *Mater. Charact.* **2005**, *55*, 43–49. [[CrossRef](#)]
237. Tavakoli, H. Investigation of tribological and physical behavior of sulfide film produced by DC -regime plasma electrolysis. *Surf. Coat. Technol.* **2017**, *309*, 1099–1104. [[CrossRef](#)]
238. Xu, S.-S.; Weng, L.-J.; Liu, Y.-Z.; Kang, K.-H.; Kim, C.-L.; Kim, D.-E. Microstructure evolution and enhanced vacuum tribological performance of Ni-doped WS₂ composite coating. *Surf. Coat. Technol.* **2017**, *325*, 81–88. [[CrossRef](#)]
239. Zhu, L.-N.; Wang, C.-B.; Wang, H.-D.; Xu, B.-S.; Zhuang, D.-M.; Liu, J.-J.; Li, G.-L. Tribological properties of WS₂ composite film prepared by a two-step method. *Vacuum* **2010**, *85*, 16–21.
240. Du, G.Y.; Ba, D.C.; Tan, Z.; Liu, K. Tribological behavior of radio-frequency sputtering WS₂ thin films with vacuum annealing. *Thin Solid Films* **2011**, *520*, 849–852. [[CrossRef](#)]
241. Yang, F.-E.; Lu, Y.; Zhang, R.; Zhang, X.-H.; Zheng, X.-H. Microstructure and tribological properties of WS_x/a-C multilayer films with various layer thickness ratios in different environments. *Surf. Coat. Technol.* **2017**, *309*, 187–194. [[CrossRef](#)]
242. Salvaro, D.; Neves, G.O.; Binder, C.; Klein, A.N.; Biasoli de Mello, J.D. Influence of SiC polytypes on the mixed lubrication regime of self-lubricating composites containing in situ generated 2D turbostratic graphite. *Tribol. Int.* **2023**, *184*, 108446. [[CrossRef](#)]
243. Li, J.; Men, S.W.; Zhang, Z.; Yang, Y.; Sun, Y.; Ding, J.C.; Wang, Q.M. Structural, mechanical, and tribological properties of GLC film on a nitrided layer prepared in a glow-discharge plasma nitriding system. *Vacuum* **2021**, *193*, 110543. [[CrossRef](#)]
244. Vergari, L.; Quincey, J.; Meric de Bellefon, G.; Merriman, T.; Hackett, M.; Scarlat, R.O. Self-lubrication of nuclear graphite in argon at high temperature. *Tribol. Int.* **2023**, *177*, 107946. [[CrossRef](#)]
245. Xie, J.; Li, J.; Fu, Q.; Wu, W.; Yang, Y.; Li, D.; Zhang, S. Graphite-like carbon films catalytically grown on a carburized substrate with an antenna structure at the interface: Experiments and first-principles calculations. *Appl. Surf. Sci.* **2023**, *639*, 158095. [[CrossRef](#)]
246. Xue, R.; Wang, J.; Zeng, Y.; Zhang, N.; Zhang, Z.; Huang, S.; Xiao, Z.; Xia, H. Self-lubrication behavior of the reaction-formed graphite/SiC composites with optimizing graphite content. *Wear* **2023**, *526–527*, 204946. [[CrossRef](#)]
247. Manu, B.R.; Gupta, A.; Jayatissa, A.H. Tribological Properties of 2D Materials and Composites—A Review of Recent Advances. *Materials* **2021**, *14*, 1630. [[CrossRef](#)]
248. Çelik, A.; Özer, H.Ö.; Tüzemen, Ş.M.; Yıldız, M.; Kovacı, H. Synthesis, characterization and tribological properties of solid lubricant graphite films produced by PECVD. *Mater. Today Commun.* **2023**, *36*, 106506. [[CrossRef](#)]
249. Kot, M.; Major, L.; Lackner, J. The tribological phenomena of a new type of TiN/a-C:H multilayer coatings. *Mater. Des.* **2013**, *51*, 280–286. [[CrossRef](#)]
250. Kasiorowski, T.; Lin, J.; Soares, P.; Lepienski, C.M.; Neitzke, C.A.; de Souza, G.B.; Torres, R.D. Microstructural and tribological characterization of DLC coatings deposited by plasma enhanced techniques on steel substrates. *Surf. Coat. Technol.* **2020**, *389*, 125615. [[CrossRef](#)]
251. Huang, Y.; Li, J.; Wang, X.; Liu, X.; Li, H.; Ren, P.; Sun, C. Tribological Properties and Corrosion Resistance of Multilayer a-C:H:Ti Films at Different Target Currents. *Metals* **2023**, *13*, 1274. [[CrossRef](#)]
252. Sola, R.; Veronesi, P.; Zardin, B.; Borghi, M. A study on PVD coatings for reduction of friction and wear of swashplate axial piston pumps and motors. *Metall. Ital.* **2020**, *3*, 14–23.
253. Rathmann, L.; Rusche, T.; Hasselbruch, H.; Mehner, A.; Radel, T. Friction and wear characterization of LIPSS and TiN/DLC variants. *Appl. Surf. Sci.* **2022**, *584*, 152654.
254. Zheng, J.; Ren, X.; Hao, J.; Li, A.; Liu, W. Carbon nanohoops as attractive toughening and lubricant agents in TiN porous films. *Appl. Surf. Sci.* **2017**, *393*, 60–66. [[CrossRef](#)]

255. Liu, G.; Wen, Z.; Chen, K.; Dong, L.; Wang, Z.; Zhang, B.; Qiang, L. Optimizing the Microstructure, Mechanical, and Tribological Properties of Si-DLC Coatings on NBR Rubber for Its Potential Applications. *Coatings* **2020**, *10*, 671. [\[CrossRef\]](#)
256. Li, A.; Chen, Q.C.; Wu, G.Z.; Wang, Y.F.; Lu, Z.B.; Zhang, G.A. Probing the lubrication mechanism of multilayered Si-DLC coatings in water and air environments. *Diam. Relat. Mater.* **2020**, *105*, 107772. [\[CrossRef\]](#)
257. Sun, H.; Yang, L.; Wu, H.; Zhao, L. Effects of Element Doping on the Structure and Properties of Diamond-like Carbon Films: A Review. *Lubricants* **2023**, *11*, 186. [\[CrossRef\]](#)
258. Ding, J.C.; Chen, M.; Mei, H.; Jeong, S.; Zheng, J.; Yang, Y.; Wang, Q.; Kim, K.H. Microstructure, mechanical, and wettability properties of Al-doped diamond-like films deposited using a hybrid deposition technique: Bias voltage effects. *Diam. Relat. Mater.* **2022**, *123*, 108861. [\[CrossRef\]](#)
259. Yan, M.M.; Wang, X.Y.; Zhang, S.W.; Zhang, S.T.; Sui, X.D.; Li, W.S.; Hao, J.Y.; Liu, W.M. Friction and wear properties of GLC and DLC coatings under ionic liquid lubrication. *Tribol. Int.* **2020**, *143*, 106067. [\[CrossRef\]](#)
260. Weicheng, K.; Zhou, Y.; Jun, H. Effect of carburizing treatment on microstructural, mechanical and tribological performances of Cr doped DLC coating deposited on Ti6Al4V alloy. *Ceram. Int.* **2021**, *47*, 34425–34436. [\[CrossRef\]](#)
261. Evaristo, M.; Fernandes, F.; Cavaleiro, A. Influence of the alloying elements on the tribological performance of DLC coatings in different sliding conditions. *Wear* **2023**, *526–527*, 204880. [\[CrossRef\]](#)
262. Brzezinka, T.L.; Rao, J.; Paiva, J.M.; Kohlscheen, J.; Fox-Rabinovich, G.S.; Veldhuis, S.C.; Endrino, J.L. DLC and DLC-WS₂ Coatings for Machining of Aluminium Alloys. *Coatings* **2019**, *9*, 192. [\[CrossRef\]](#)
263. Fiaschi, G.; Rota, A.; Ballestrazzi, A.; Marchetto, D.; Vezzalini, E.; Valeri, S. A Chemical, Mechanical, and Tribological Analysis of DLC Coatings Deposited by Magnetron Sputtering. *Lubricants* **2019**, *7*, 38. [\[CrossRef\]](#)
264. Shen, Y.; Liao, B.; Zhang, Z.; Wu, X.; Ying, M.; Zhang, X. Anti-sand erosion and tribological performance of thick DLC coatings deposited by the filtered cathodic vacuum arc. *Appl. Surf. Sci.* **2020**, *533*, 147371. [\[CrossRef\]](#)
265. Beake, B.D.; McMaster, S.J.; Liskiewicz, T.W.; Neville, A. Influence of Si- and W- doping on micro-scale reciprocating wear and impact performance of DLC coatings on hardened steel. *Tribol. Int.* **2021**, *160*, 107063. [\[CrossRef\]](#)
266. Vahidi, A.; Fonseca, D.; Oliveira, J.; Cavaleiro, A.; Ramalho, A.; Ferreira, F. Advanced Tribological Characterization of DLC Coatings Produced by Ne-HiPIMS for the Application on the Piston Rings of Internal Combustion Engines. *Appl. Sci.* **2021**, *11*, 10498. [\[CrossRef\]](#)
267. Li, N.; Wang, M.C.; Wu, Z.G. Mass-Produced Cu Nanoparticles as Lubricant Additives to Enhance the Tribological Properties of DLC Coatings. *Metals* **2022**, *12*, 1350. [\[CrossRef\]](#)
268. Wang, F.; Wang, L.; Xue, Q. Fluorine and sulfur co-doped amorphous carbon films to achieve ultra-low friction under high vacuum. *Carbon* **2016**, *96*, 411–420. [\[CrossRef\]](#)
269. Farfan-Cabrera, L.I.; Cao-Romero-Gallegos, J.A.; Lee, S.; Komurlu, M.U.; Erdemir, A. Tribological behavior of H-DLC and H-free DLC coatings on bearing materials under the influence of DC electric current discharges. *Wear* **2023**, *522*, 204709. [\[CrossRef\]](#)
270. Li, Q.; Huang, T.; Yang, M.; Gao, T.; Ji, B.; Zhang, S.; Zhang, L.; Tu, R. Effects of gradient structure and modulation period of Ta/TaN/Ta(C,N)/Ta-DLC multilayer coatings prepared by HiPIMS. *Surf. Coat. Technol.* **2023**, *459*, 129406. [\[CrossRef\]](#)
271. Zhang, J.; Wang, Y.; Zhou, S.; Wang, Y.; Wang, C.; Guo, W.; Lu, X.; Wang, L. Tailoring self-lubricating, wear-resistance, anticorrosion and antifouling properties of Ti/(Cu, MoS₂)-DLC coating in marine environment by controlling the content of Cu dopant. *Tribol. Int.* **2020**, *143*, 106029. [\[CrossRef\]](#)
272. Zhao, J.; Gao, T.; Li, Y.; He, Y.; Shi, Y. Two-dimensional (2D) graphene nanosheets as advanced lubricant additives: A critical review and prospect. *Mater. Today Commun.* **2021**, *29*, 102755. [\[CrossRef\]](#)
273. Wu, P.; Chen, X.; Zhang, C.; Luo, J. Synergistic tribological behaviors of graphene oxide and nanodiamond as lubricating additives in water. *Tribol. Int.* **2019**, *132*, 177–184. [\[CrossRef\]](#)
274. Jin, B.; Zhao, J.; Chen, G.; He, Y.; Huang, Y.; Luo, J. In situ synthesis of Mn₃O₄/graphene nanocomposite and its application as a lubrication additive at high temperatures. *Appl. Surf. Sci.* **2021**, *546*, 149019. [\[CrossRef\]](#)
275. Zhao, J.; Mao, J.; Li, Y.; He, Y.; Luo, J. Friction-induced nano-structural evolution of graphene as a lubrication additive. *Appl. Surf. Sci.* **2018**, *434*, 21–27. [\[CrossRef\]](#)
276. Luo, B.; Zhou, H.; Liu, D.; Luo, F.; Tian, Y.; Chen, D.; Wei, W. One-step in-situ reaction synthesis of TiC/graphene composite thin film for titanium foil surface reinforcement. *Vacuum* **2019**, *160*, 472–477. [\[CrossRef\]](#)
277. Yu, Y.; Tian, H.; Wang, C.; Tang, Z.; Gao, J. Effect of graphene content on properties of self-lubrication and wear resistant GO/WC-Co coating. *Heat Treatment. Met.* **2018**, *43*, 173–178.
278. Wang, J.; Zhang, K.; Zhang, L.; Wang, F.; Zhang, J.; Zheng, W. Influence of structure evolution on tribological properties of fluorine-containing diamond-like carbon films: From fullerene-like to amorphous structures. *Appl. Surf. Sci.* **2018**, *457*, 388–395. [\[CrossRef\]](#)
279. Wang, Y.; Ling, X.; Wang, Y.; Zhang, J. Probing the effect of doped F and N on the structures and properties of fullerene-like hydrogenated carbon films. *Diam. Relat. Mater.* **2017**, *79*, 32–37. [\[CrossRef\]](#)
280. Flores-Ruiz, F.J.; Enriquez-Flores, C.I.; Chiñas-Castillo, F.; Espinoza-Beltrán, F.J. Nanotribological performance of fullerene-like carbon nitride films. *Appl. Surf. Sci.* **2014**, *314*, 193–198. [\[CrossRef\]](#)
281. Wang, P.; Wang, X.; Zhang, B.; Liu, W. Formation of hydrogenated amorphous carbon films containing fullerene-like structures. *J. Non-Cryst. Solids* **2009**, *355*, 1742–1746. [\[CrossRef\]](#)

282. Wang, Y.; Guo, J.; Gao, K.; Zhang, B.; Liang, A.; Zhang, J. Understanding the ultra-low friction behavior of hydrogenated fullerene-like carbon films grown with different flow rates of hydrogen gas. *Carbon* **2014**, *77*, 518–524. [[CrossRef](#)]
283. Wang, Y.; Yue, Z.; Wang, Y.; Zhang, J.; Gao, K. Synthesis of fullerene-like hydrogenated carbon films containing iron nanoparticles. *Mater. Lett.* **2018**, *219*, 51–54. [[CrossRef](#)]

Disclaimer/Publisher’s Note: The statements, opinions and data contained in all publications are solely those of the individual author(s) and contributor(s) and not of MDPI and/or the editor(s). MDPI and/or the editor(s) disclaim responsibility for any injury to people or property resulting from any ideas, methods, instructions or products referred to in the content.